FRERES MENTOURI UNIVERSITY
CONSTANTINE 1 -ALGERIA

Journal of Sciences & Technology

Semestrial Journal of Freres Mentouri University, Constantine, Algeria

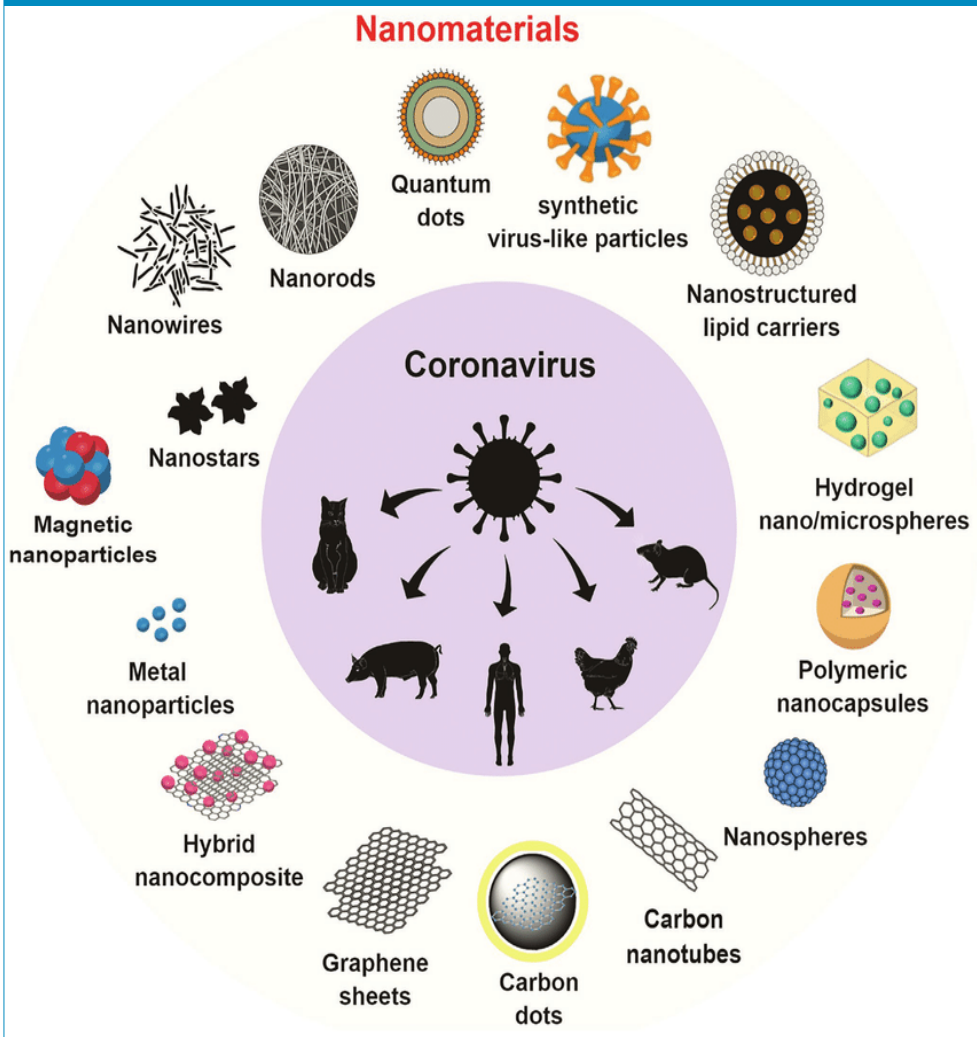

VOLUME 06 - ISSUE 01— JUNE 2021

EISSN: ….-….

Freres Mentouri University Constantine

Ain El-Bey Road
Constantine 25000
Algeria

Phone.Fax: 213 (0) 31. 81. 12.78
Email: revues@umc.edu.dz
Website :http://revue.umc.edu.dz

Journal of Sciences & Technology

Volume 6 N° 1 June 2021

Semestrial Journal of Freres Mentouri University
Constantine, Algeria

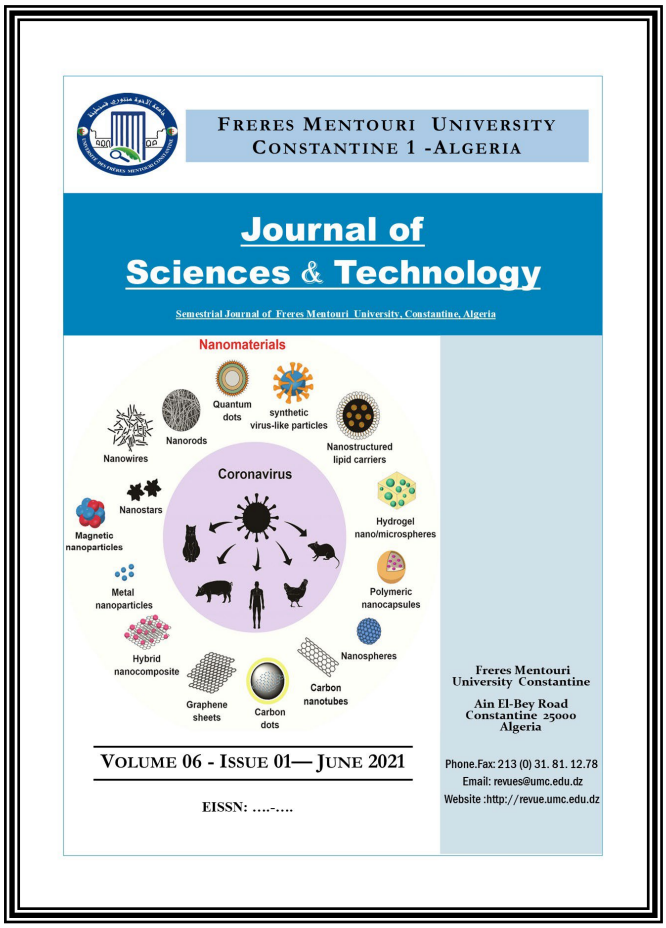

SOUMISSION DES ARTICLES

An article proposed for publication should not be submitted at the same time to another journal.

Manuscripts (original and two copies) should be sent to the following address:

Vice-Rectorate in charge of Post-Graduation and Scientific Research

Direction of Publications and Scientific Animation (15th floor)

Constantine 1 University , Aïn-El-Bey Road, 25000 Constantine, ALGERIA.

Tél./Fax: 213 (0) 31.81.12.78

e-mail: revues@umc.edu.dz

Freres Mentouri Constantine 1 University

Journal of Sciences & Technology

Volume 6 N° 1 – June 2021

SCIENTIFIC COMMITTEE

INSTRUCTIONS TO AUTHORS

I- Overview

The journal Human Sciences publishes in three languages: Arabic, French and English. Two abstracts must be provided, one in the language of the article, the other in Arabic if the article is written in another language, or in French (or English) if the article is written in Arabic. Abstracts must not exceed 150 words. Unpublished articles are not returned to their authors.

II- Manuscrips

The articles submitted for publication (three copies) must not exceed 20 typewritten pages (tables, figures, graphs, bibliography, ... included) with a large margin to the left (3 cm), printed on 21 x 29 paper , 7 cm (A4) with interligne of good readability. Some flexibility is allowed to authors, but they should organize the text clearly in sections such as: Introduction, Experimental Details, Results, Discussion and Conclusion. The longer articles will be published by part in successive issues, each part being determined by the authors. Authors are kindly requested to accompany the summary of their articles with the most complete possible keywords.

In order to save time and respect deadlines for publication, it is recommended that authors take care of the complete capture of their article on a computer, and send it to the journal, after they have been informed. acceptance for publication, in the form of files on CD.ROM, which will be copied by the service.

However, since the final formatting of the article is done by P.A.O. (Computer Aided Publication), the authors are asked to avoid any formatting of their text. It will be necessary to avoid stylizing it.

III- Bibliography

The bibliographic references quoted in the text must include only the reference number in square brackets (ex .: [5]). If the name of the author appears in the text, it must be followed by the reference number. When the reference contains more than two authors, only the first is cited, followed by "and al".

For articles, the complete reference includes the names of the authors followed by the initials of their first names, the title of the article, the title of the periodical (in conformity with the abbreviations allowed), the volume, the number of the periodical, the year of publication and the relevant pages.

For the works, the reference must include the names of the authors followed by the initials of their first names, the complete title of the work, the volume, the volume, the first and the last page relating to the results discussed, the number of the edition if there are several, the name of the publisher, the place and the year of edition.

For scientific meetings (congresses, proceedings, ...), the reference includes the names of the authors followed by the initials of their first names, the title of the communication, the identification of the meeting, the place, the period and the pages concerned.

IV- Iconography

Tables, boards, charts, maps, photographs, etc. must be provided separately, inset. They must be presented on white sheets of A4 format, individually or in groups, and have underneath the words "table" or "figure" assigned a number.

The illustrations and figures must be clear, professionally made and adequate for reproduction: a 50% reduction, if any, must lead to a suitable size and thickness of characters for good readability. Moreover, for computer-generated figures, in order to maximize contrast, the use of a laser or inkjet printer is essential.

Legends assigned their numbers must be grouped in a separate page.

The final presentation of the article will be left to the discretion of the Editorial Board.

Journal of Sciences & Technology
Volume 6 N° 1– June 2021

SUMMARY

SUMMARY

Journal of Sciences & Technology
Volume 6 N° 1– June 2021

LAMB SHIFT IN HYDROGEN-LIKE ATOM INDUCED FROM NON-COMMUTATIVE QUANTUM SPACE-TIME

Submited on 02/05/2012 – Accepted on 24/06/2014

Abstract

In this work we present an important contribution to the non-commutative approach to the hydrogen atom to deal with lamb shift corrections. This can be done by studying the Klein-Gordon equation in a non-commutative space-time as applied to the Hydrogen atom to extract the energy levels, by considering the second-order corrections in the non commutativity parameter and by comparing with the result of the current experimental results on the Lamb shift of the 2P level to extract a bound on the parameter of non-commutativity. Phenomenologically we show that the non-commutativity effects induce lamb shift corrections.

Keywords: *Klein-Gordon equation, non-commutative space, quantum Hydrogen atom.*

S ZAIM
H EGLMMAMNE

Department of Physics, Faculty of Sciences of Matter, University of Batna 1, Algeria.

I. INTRODUCTION

In recent years many arguments have been suggested to motivate a deviation from the flat-space concept at very short distances [1, 2] so that we have a new concept of quantum spaces. Quantum spaces depend on parameters such that for a particular value of these parameters they become the usual flat space. We consider the simplest version of quantum spaces as the natural extension of the usual quantum mechanical commutation relations between position and momentum, by imposing further commutation relations between position coordinates themselves. The non-commutative space can be obtained by the coordinate operators where we replace the ordinary product by star product: $\left[x^{\mu}, x^{\nu}\right] = i\theta^{\mu\nu}$

Our motivation is to study the effect of non-commutativity at the level of quantum mechanics when time-space non-commutativity is accounted for. One can study the physical consequences of this theory by making detailed analytical estimates for measurable physical quantities and compare the results with experimental data to find an upper bound on the θ parameter. In this work we present an important contribution to the non-commutative approach to the hydrogen atom. Our goal is to solve the Klein-Gordon equation for the Coulomb potential in a non-commutative space-time up to second-order in the non-commutativity parameter using the Seiberg-Witten maps and the Moyal product. We thus find the non-commutative modification of the energy levels of the hydrogen atom and we show that the non-commutativity is the source of lamb shift corrections.
The purpose of this paper is to study the extension of the Klein-Gordon field in canonical non- commutative time-space by applying the result obtained to a hydrogen atom. This paper is organized as follows. In section 2, we propose an invariant action of the non-commutative boson field in the presence of an electromagnetic field. In section 3, using the generalised Euler-Lagrange field equations, we derive the deformed Klein-Gordon (KG) equation for the hydrogen atom. We solve these deformed equation and obtain the noncommutative modification of the energy levels. Furthermore, we derive the nonrelativistic limit of the non-commutative KG equation for a hydrogen atom and solve it using perturbation theory. Finally, in section 4, we draw our conclusions.

II. ACTION

We consider an action for a free boson field in the presence of electrodynamic gauge field in a non-commutative space-time. We propose the following action [28].

$$S = \int d^4x \left(L_{MB} - \frac{1}{4} F_{\mu\nu} * F^{\mu\nu} \right) \tag{1}$$

Where $\mathrm{L_{MB}}$ is the boson matter densitie in the non-commutative space-time and is given by:

$$L_{MB} = \eta^{\mu\nu} (\hat{D}_{\mu} \hat{\varphi})^{+} * (\hat{D}_{\nu} \hat{\varphi}) + m^2 \hat{\varphi}^{+} * \hat{\varphi} \tag{2}$$

where the gauge covariant derivative is defined as:

$\hat{\mathrm{D}}_{\mu} = \partial_{\mu} + ie\hat{A}_{\mu}$.

From the action variational principle the generalised equations of Lagrange up to second order of θ are [29]:

$$\frac{\partial L}{\partial \hat{\varphi}} - \partial_{\mu} \frac{\partial L}{\partial (\partial_{\mu} \hat{\varphi})} + \partial_{\mu}\partial_{\nu} \frac{\partial L}{\partial (\partial_{\mu}\partial_{\nu} \hat{\varphi})} + \mathrm{O}(\theta^2) = 0 \tag{3}$$

Where:

$$L = L_{MB} - \frac{1}{4} F_{\mu\nu} * F^{\mu\nu} \tag{4}$$

III. NON-COMMUTATIVE TIME-SPACE KG EQUATION

Using the modified field equation (3) , with the generic boson field $\hat{\varphi}$ one can find in a free non-commutative space-time and in the presence of the external potential $\hat{A}_\mu$ the following modified Klein-Gordon equation:

$$\left(\eta^{\mu\nu}\partial_\mu\partial_\nu - m_e{}^2\right)\hat{\varphi} + \left(ie\eta^{\mu\nu}\partial_\mu\hat{A}_\nu - e^2\eta^{\mu\nu}\hat{A}_\mu * \hat{A}_\nu + 2ie\eta^{\mu\nu}\hat{A}_\mu\partial_\nu\right)\hat{\varphi} = 0 \tag{5}$$

Where the deformed external potential $\hat{A}_\mu\begin{pmatrix}-e/r\\0\end{pmatrix}$ in free non-commutative space-time is [30]:

$$\hat{a}_0 = -\frac{e}{r} - \frac{e^3}{r^4}\theta^{0k}x_k + \mathrm{O}(\theta^2).$$
$$\hat{a}_i = \frac{e^3}{4r^4}\theta^{ik}x_k + \mathrm{O}(\theta^2) \tag{6}$$

for a non-commutative time-space, $\theta^{0k} \neq 0$ and $\theta^{ik} = 0$, where i; k = 1; 2; 3. In this case, we can check that

$$\eta^{\mu\nu}\partial_\mu\partial_\nu = -\partial_0{}^2 + \Delta \tag{7}$$

And

$$2ie\eta^{\mu\nu}\hat{A}_\mu\partial_\nu = i\frac{2e^2}{r}\partial_0 + 2i\frac{e^4}{r^4}\theta^{0j}x_j\partial_0$$
$$-e^2\eta^{\mu\nu}\hat{A}_\mu * \hat{A}_\nu = \frac{e^4}{r^2} + 2\frac{e^5}{r^5}\theta^{0j}x_j \tag{8}$$

then the Klein-Gordon equation (20) up to $\mathrm{O}(\theta^2)$ takes the form:

$$\left(-\partial_0{}^2 + \Delta - m_e{}^2\right)\hat{\varphi} + \left(\frac{e^4}{r^2}{}_\nu + i\frac{2e^2}{r}\partial_0 + 2i\frac{e^4}{r^4}\theta^{0j}x_j\partial_0 + 2\frac{e^5}{r^5}\theta^{0j}x_j\right)\hat{\varphi} = 0 \tag{9}$$

The solution to eq. (9) in spherical polar coordinates (r,ϑ,ϕ) takes the separable form:

$$\hat{\varphi}(r,\vartheta,\phi,t) = \frac{1}{r}\,\hat{\mathrm{R}}(\mathrm{r})\hat{Y}(\vartheta,\phi)\exp(-iEt) \tag{10}$$

Then eq. (9) reduces to the radial equation:

$$\left(\frac{d^2}{dr^2} - \frac{l(l+1)-e^4}{r^2} + \frac{2Ee^2}{r}\right)\hat{R} + \left(E^2 - m_e^2 + 2E\frac{e^4}{r^4}\theta^{0j}x_j + 2\frac{e^5}{r^5}\theta^{0j}x_j\right)\hat{R} = 0 \tag{11}$$

In eq.(11) the coulomb potential in non-commutative space-time appears within the perturbation terms [31]:

$$H^{\theta}_{pert} = 2E\frac{e^4}{r^4}\theta^{0j}x_j + 2\frac{e^5}{r^5}\theta^{0j}x_j, \tag{12}$$

where the first term is the electric dipole–dipole interaction created by the non-commutativity, the second term is the electric dipole–quadruple interaction. These interactions show us that the effect of space-time non-commutativity on the interaction of the electron and the proton is equivalent to an extension of two nuclei interactions at a considerable distance. This idea effectively confirms the presence of gravity at this level. To investigate the modification of the energy levels by eq. (12), we use the first-order perturbation theory. The spectrum of H_O and the corresponding wave functions are well-known and given by:

$$R_{nl}(r) = \sqrt{\frac{a}{n+\nu+1}}\left(\frac{n!}{\Gamma(n+2\nu+2)}\right)^{1/2} x^{\nu+1} .e^{-x/2}L_n^{2\nu+1}(x). \tag{13}$$

where the relativistic energy levels are given by:

$$E_{nl}{}^0 = \frac{m_e\left(n_{+1/2} + \sqrt{(l_{+1/2})^2 - \alpha^2}\right)}{\sqrt{(n_{+1/2})^2 + (l_{+1/2})^2 + 2n_{+1/2}\sqrt{(l_{+1/2})^2 - \alpha^2}}} \tag{14}$$

and $L_n^{2\nu+1}$ are the associated Laguerre polynomials [32], with the following notations:

$$\nu = -\frac{1}{2} + \sqrt{(l_{+1/2})^2 - \alpha^2},\ \alpha = e^2,$$
$$a = \sqrt{m_e^2 - E_{nl}^{02}}$$
$$n_{+1/2} = n + 1/2,\ l_{+1/2} = l + 1/2 \tag{15}$$

III. 1 NON-COMMUTATIVE CORRECTIONS OF THE RELATIVISTIC ENERGY

Now to obtain the modification to the energy levels as a result of the terms (12) due to the non-commutativity of space-time we use perturbation theory. For simplicity, first of all, we choose the coordinate system (t,r,ϑ,ϕ) so that $\theta^{0i} = -\theta^{i0} = \theta\delta^{01}$; such that $\theta^{0i}x_i = \theta r$ and assume that the other components are all zero and also the fact that in first-order perturbation theory the expectation value of r^{-3} and r^{-4} are as follows:

$$\left\langle nlm\middle|r^{-3}\middle|nlm'\right\rangle = \int_0^\infty R_{nl}^2 r^{-1}dr\delta_{mm'}$$
$$= \frac{2a^3}{\nu(2\nu+1)(n+\nu+1)}\left[1 + \frac{n}{\nu+1}\right]\delta_{mm'} \tag{16}$$
$$= f(3)$$

$$\left\langle nlm\left|r^{-4}\right|nlm'\right\rangle = \int_0^\infty R_{nl}^2 r^{-2} dr \delta_{mm'}$$
$$= \frac{4a^4}{(2\nu-1)\nu(2\nu+1)(n+\nu+1)}\left\{1+\frac{3n}{\nu+1}\right. \quad (17)$$
$$\left.+\frac{3n(n-1)}{(\nu+1)(2\nu+3)}\right\}\delta_{mm'} = f(4),$$

Now, the correction to the energy to first order in Theta is:

$$E^{\theta(1)} = \left\langle H_{pert}^{\theta}\right\rangle_{nlm} \quad (18)$$

wher H_{pert}^{θ} is the non-commutative corrections perturbation Hamiltonian, which is given in the following relation:

$$H_{pert}^{\theta} = 2E\frac{e^4}{r^3}\theta + 2\frac{e^5}{r^4}\theta \quad (19)$$

To calculate $E^{\theta(1)}$, we use the results in equations (16) and (17), to obtain:

$$E^{\theta(1)} = 2\theta\alpha^2\left[E_{nl}^0 f(3) + \alpha f(4)\right] \quad (20)$$

Finally the energy correction of the hydrogen atom in the framework of the non-commutative KG equation is:

$$\Delta E^{NC} = \frac{E^{\theta(1)}}{2E_{nl}^0} = \theta\alpha^2\left[f(3)+\frac{\alpha}{E_{nl}^0}f(4)\right] \quad (21)$$

This result is important because it reflects the existence of Lamb shift, which is induced by the non-commutativity of the space. Obviously, when $\theta = 0$; then $\Delta E^{NC} = 0$, which is exactly the result of the space-space commuting case, where

the energy-levels are not shifted. We showed that the energy-level shift for 1S is:

$$\Delta E_{1S}^{NC} = \theta\alpha^2\left[f_{1S}(3)+\frac{\alpha}{E_{10}^0}f_{1S}(4)\right] \quad (22)$$

In out analysis, we simply identify spin up if the non-commutativity parameter takes the eigenvalue $+\theta$ and spin down if non-commutativity parameter takes the eigenvalue $-\theta$. Also we can say that the Lamb shift is actually induced by the space-time non-commutativity which plays the role of a magnetic field and spin in the same moment (Zemann effect). This represents Lamb shift corrections for $l = 0$. This result is very important: as a possible means of introducing electron spin we replace $l \to \pm(j+1/2)$ and $n \to n-j-1-1/2$ where j is the quantum number associated to the total angular momentum.

Then the $l = 0$ state has the same total quantum number $j = 1/2$. In this case the non-commutative value of the energy levels indicates the splitting of $1S$ states.

III.2 NON-RELATIVISTIC LIMIT

The non-relativistic limit of the non-commutative K-G equation (11) is written as [33, 34]:

$$\left(\frac{d^2}{dr^2} - \frac{l(l+1)-e^4}{r^2} + \frac{2m_e e^2}{r} + 2m_e\varepsilon\right.$$
$$\left. + 2m_e\frac{e^4}{r^3}\theta + 2\frac{e^5}{r^4}\theta\right)\hat{R} = 0 \quad (23)$$

In this non-relativistic limit the charged boson does not represent a single charged particle, but is a distribution of positive and negative charges which are different and extended in space linearly in $\sqrt{\theta}$. The absence of a perturbation term of form θ/r^2 in the non-commutative coulomb interaction demonstrates that the distribution of positive and negative charges is spherically symmetric.
This can be interpreted as the spherically symmetric distribution of charges of the quarks inside in the proton.
Now to obtain the modification of energy levels as a result of the non-commutative terms in eq. (23), we use the first-order perturbation theory. The spectrum of $H_0(\theta = 0)$ and the corresponding wave functions are well-known and given by:

$$\varepsilon_n = \frac{m_e\alpha^2}{2\hbar^2 n^2} \quad (24)$$

And

$$R_{nl}(r) = \frac{1}{n}\left(\frac{(n-l-1)!}{a(n+l)!}\right)^{1/2} x^{l+1}e^{-x/2}L_{n-l-1}^{2l+1}(x). \quad (25)$$

where $x = \frac{2r}{an}$ and $a = \hbar^2/(m_e\alpha)$ is the Bohr radius of the Hydrogen atom. The coulomb potential in non - commutative space-time appears within the perturbation terms:

$$H_{pert}^{\theta} = 2\theta\alpha^2\left(\frac{m_e}{r^3}+\frac{\alpha}{r^4}\right) \quad (26)$$

where the expectation value of r^{-3} and r^{-4} are as follows:

$$\left\langle nlm\left|r^{-3}\right|nlm'\right\rangle_{l>0} = \frac{2}{a^3n^3l(l+1)(2l+1)}\delta_{mm'} \quad (27)$$
$$= g(3)$$
$$\left\langle nlm\left|r^{-4}\right|nlm'\right\rangle_{l>0} = \left\{\frac{4(3n^3-l(l+1))}{a^4n^5(2l-1)l(l+1)(2l+1)(2l+3)}\right.$$
$$\left.+\frac{35(3n^3-l(l+1))}{3(l-1)(2l-1)(l+2)(2l+1)(2l+3)}\right\}\delta_{mm'}$$
$$= g(4) \quad (28)$$

Hence the modification to the energy levels is given by:

$$\Delta E^{NC} = \theta\alpha^2\left[g_{nl}(3) + \frac{\alpha}{m_e}g_{nl}(4)\right] + \mathrm{O}\left(\theta^2\right) \qquad (29)$$

We can also compute the correction to the Lamb shift of the 2P level where we have:

$$\Delta E^{NC}\left(2P\right) = 0.243156\theta\left(MeV\right)^3 \qquad (30)$$

According to ref. [35] the current theoretical result for the lamb shift is 0:08 kHz. From the splitting (30), this then gives the following bound on θ:

$$\theta \le \left(8.5TeV\right)^{-2} \qquad (31)$$

This corresponds to a lower bound for the energy scale of $8.5TeV$, which is in the range that has been obtained in refs [36, 37, 38, 39], namely $1-10TeV$.

IV. CONCLUSION

Using the Seiberg-Witten maps and the Moyal product up to second order in the non-commutativity parameterθ, we have derived the deformed KG equation for a hydrogen atom in non-commutative space-time. By solving the deformed KG equation we found the energy shift up to the second order of θ, which proofs that the non-commutativity has an effect similar to that of the Lamb Shift. After that we have obtained the non-relativistic limit of the non-commutative KG equation for a Coulomb potential. We then compared the corrections induced to energy levels by this non-commutative effect to experimental results from high precision hydrogen spectroscopy, and obtained the bound for the parameter of non-commutativity around $\left(8.5TeV\right)^{-2}$.

ACKNOWLEDGMENT

I am grateful to Zeroual Aouachria for useful discussions and suggestions." **This work is supported by the CNEPRU project: D01320130009.**

REFERENCES

[1] S. Doplicher, K. Fredenhagen and J.E. Roberts, Phys. Lett. B331, 39

(1994).

[2] S. Doplicher, K. Fredenhagen and J.E. Roberts, Commun. Math. Phys.

172, 187 (1995).

[3] S. Zaim, A. Boudine, N. Mebarki, M. Moumni, Rom. Journ. Phys., Vol. 53, Nos. 3–4, P. 445–462 (2008).

[4] N. Mebarki, S. Zaim, L Khodja and H Aissaoui Phys. Scripta 78 045101(2008).

[5] A. Stern Phy. Rev. Lett. 100 061601 (2008).

[6] S. Zaim and Y. Delenda J. Phys. Conf. Ser.435 012020(2013).

[7] A. F. Nikiforov and V. B. Uvarov Special Functions of Mathematical

Physics (Basel: Birkhauser) (1988).

[8] M. R. Setareand and O. Hatami Commun. Theor. Phys. (Beijing) 51, 1000 (2009).

[9] S. Zaim, L. Khodja and Y. Delenda Int. J. Mod. Phys. A 26 4133 (2011).

[10] C. Itzykson and J.-B. Zuber, Quantum Field Theory, Dover Publications, New York, (2005).

[11] M. Chaichian, M. M. Sheikh-Jabbari and A. Tureanu Phys. Rev. Lett. 86 2716 (2001).

[12] J.L. Hewett, F.J. Petriello, T.G. Rizzo Phys. Rev. D64 075012 (2001).

[13] *Letter Symbols for Quantities*, ANSI Standard Y10.5-1968.

[14] S. M. Carroll, J. A. Harvey, V. A.Kostelecky, C. D. Lane,T. Okamoto Phys. Rev. Lett. 87 141601 (2001).

[15] I. Mocioiu, M. Pospelov, R. Roiban Phys. Lett. B489 390 (2000).

EDDY CURRENT CHARACTERIZATION OF NANOMATERIALS

Submited on 17/08/2014 – Accepted on 11/05/2015

Abstract

NDT Magnetic measurements as impedance in Eddy currents, corecitif and residual field in hysteresis loop are used to study the different stages of mechanical alloying in the Fe–Co system. In this paper, we changed the electromagnetic properties of Fe-Co, by developing their metallurgical parameters such as grain size. For this we are used a planetary ball mill, we are milled the FeCo alloy for different milling times until to obtain nanostructure, the lamellar structure with some small particles embedded in them was observed during the first stage of mechanical alloying. XRD patterns show after 10 h of milling the formation of a disordered solid solution having a body-centered cubic (bcc) structure. After 40h of milling, morphological studies indicated that the average crystallites size is around 15 nm.

Mots clés: *nanostructured materials, powder metallurgy, NDT, Eddy current, Magnetic measurement.*

A YOUNES [1]
N BACHA [2]
M ZERGOUG [2]
H OUBOUCHOU [2]

1 Research Center in Industrial Technologies CRTI, ex-CSC, Cheraga , Algiers- Algeria.

2 Laboratory of surface treatment & Materials, University of Saad Dahleb Blida, Algeria.

I. INTRODUCTION

In Recent years, we have witnessed a considerable development in nanomaterials science and technology. Nanomaterials were elaborated thanks to varied ways, and high-energy mechanical alloying is one technique that has many potentialities of application, the ability to control the nonstructural components is an important factor and gives important information's about in engineering developments. The characterization of microstructures, mechanical properties, deformation, damage initiation and growth by Non-Destructive Evaluation (NDE) techniques plays a vital role in various industries because of the growing awareness of the benefits that can be derived by using NDE techniques for assessing the performance of various components. In this study we apply NDT methods to characterize the nanostructure [1-8].

II. RESULTS

1. Eddy Current measurement

The analysis of Eddy Current shows that we can determine the status of nano structural by analyzing the impedance diagram [9-10].
The impedance diagram for each sample studied is different. This corresponds to a change of microstructure during milling, see Fig.1:

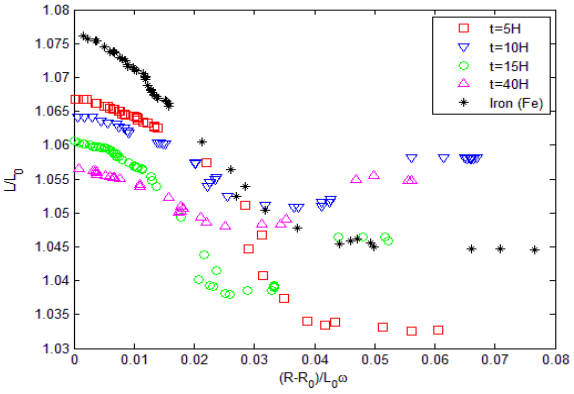

- Iron has a high impedance compared to Fe-Co
- For Fe-Co, the milling time influences the impedance diagrams; we note that when the frequency increases, a narrowing of the trajectories is obtained.

The curve is very important because we can see through the trajectories of the impedance diagram that the material obtained during milling loses its magnetic qualities stored according to the presence of Cobalt. For the nanostructure we have shown the relationship between impedance, crystallite size and lattice parameters.

Fig.2. illustrates the evolution of the impedance (Z) and crystallite size versus milling time in high frequency. The evolution of the impedance decreases in the same way of the curve representing the crystallite size.

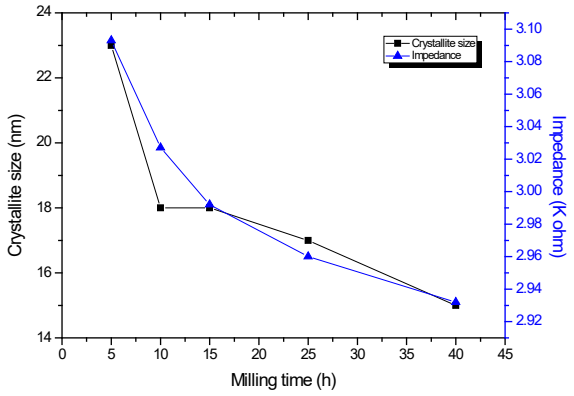

The evolution of the impedance (Z) and crystallite size versus milling time at 4862Hz frequency follows the same evolution, Fig. 2.

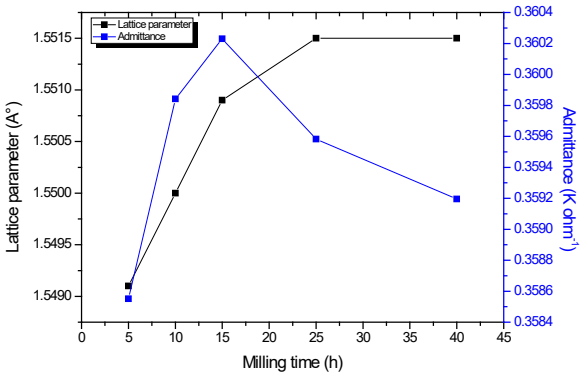

Fig.3. illustrates the evolution of the admittance and lattice parameters versus milling time in low frequency. The evolution of the admittance increases in the same way of the curve representing the Lattice parameter.
The evolution of the admittance and lattice parameter versus milling time at 1000Hz frequency has the same evolution, Fig. 3.

2. Magnetic Measurement

The coercivity is often seen as an important parameter if low losses are to be achieved. We were tried to find the relationship between the coercivity and microstructure of magnetic alloys [11, 14].

Fig.4. illustrates the evolution of the coercivity and the residual field versus milling time. As shown in Fig.5, the residual field shows a maximum value and the coercivity is a minimum value respectively at 5 hours of milling. The intersection of two curves at 15 h represented the appearance of FeCo alloy.

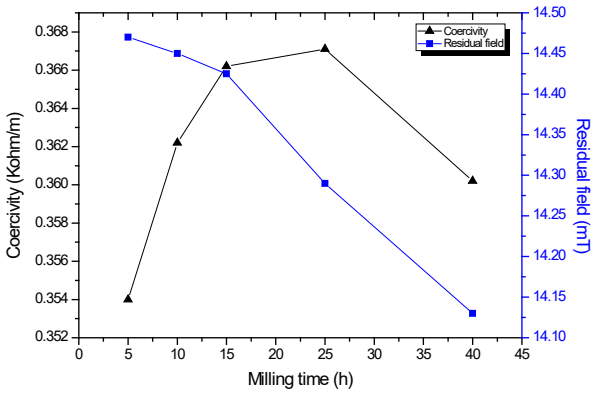

Fig.5. illustrates the evolution of the coercivity and lattice parameters versus millig time. The evolution of the coercivity increases in the same way of the curve representing the lattice parameter. As for soft magnetic systems in general, the coercivity of FeCo alloys depends strongly on the microstructure.

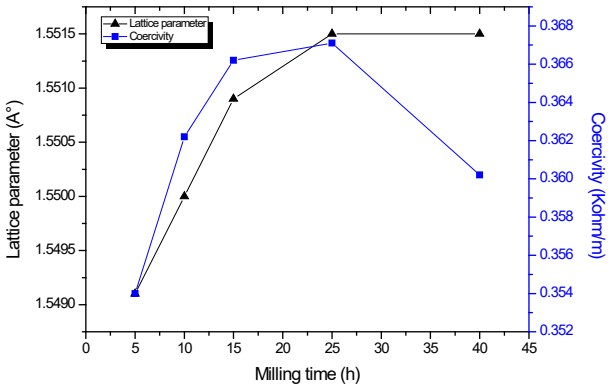

III. CONCLUSION

We can analyze the material nanostructured elaborated by mechanical alloying by NDT electromagnetic methods. The reduction of grain size enhanced the magnetic and mechanical property of FeCo alloys.
The coercivity of FeCo alloy depends strongly on the microstructure, the residual field and the coercivity shows a maximum and minimum value respectively at 5 hours of milling, the evolution of the coercivity increases in the same way as the curve representing the lattice parameters
It is possible to characterize the nanomaterials by the electromagnetic method (eddy currents).
The results are obtained:

- the evolution of the crystallite size have the same behavior of impedance
- the evolution of the lattice parameter have the same behavior of admittance

REFERENCES

[1]. C. Suryanarayana, E. Ivanov and V.V.Boldyrev,Materials Sci. and Eng. A304–306, 151–158 (2001).

[2]. J.S. Benjamin, Metallurgical Transaction 1 2943 (1970). 3.

[3]. Karimi L., Shokrollahi H., (2011) j.Alloys Compd., 509, pp.6571-6577. Applied Sciences 6 (4),

[4]. T. Sourmail, Prog. Mater. Sci. 50 (2005) 816–880.

[5]. R.H. Yu, S. Basu, R.Y. Zhang, A. Parvizi-Marjidi, IEEE Trans Magn 36(5) (2000) 388–93.

[6]. Lesile-Pelecky, D.L. Rieke, R.D. (1996), ‘’Magnetic properties of nanostructured materials’’, Chem. Mater. 8 (8) 1770–1783.

[7]. Herzer. G. (1996) Nanocrystalline soft magnetic materials, J. Magn. Magn. Mater. 157/158 133–136.

[8]. Gleiter H. (1995) Nanostructured materials: state of the art and perspective, Nanostruct. Mater. 6) 3–14.

[9]. M.Zergoug, H.Oubouchou and N.Amimeur, American J. of Applied Sciences 6 (4), 752-756. (2009).

[10]. Yu R.H., Basu S., Zhang Y. Xiao J.Q, (2000) Magnetic domains and coercivity in FeCo soft magnetic alloys, J. Appl. Phys. 85 (8) 6034–6036.

[11]. Fecht H.J., (1995) Nanostructure formation by mechanical attrition, Nanostruct. Mater. 6 33–42.

[12]. O’Handley RC. (2000) Modern magnetic materials (principles and applications). Wiley– Interscience, p. 367.

[13]. Bahrami A, Madaah Hosseini HR. (2005) Preparation of nanocrystalline Fe–Si–Ni soft magnetic powders by mechanical alloying. Mater Sci Eng B;123:74.

[14]. Turgut Z., Scott, J.H.M.Q. Huang, Majetich S.A., Mchenry M.E., (1998)Magnetic properties and ordering in C-coated FexCo1 x alloy nanocrystals, J. Appl. Phys. 83 (11) 6468–6470.

EVALUATION OF SIZE AND SHAPE OF THE SILVER NANOPARTICLES PREPARED BY CHEMICAL SYNTHESIS FOR THERAPEUTIC APPLICATIONS.

Submitted on 10/02/2018 – Accepted on 04/11/2018

Abstract

The silver nanoparticles are known such as diffusers and efficient light absorbers, because of their strong interactions with visible light through the phenomenon of surface Plasmon resonance (SPR). Local frequency LSPR strongly depends on the size, shape and dielectric medium. The synthesis of silver nanoparticles of different sizes was carried out, using different molar concentrations of silver nitrate at different temperatures in two different solvents (ethanol and methanol). the synthesized nanoparticles were characterized by UV-Visible spectroscopy. The results show the presence of an absorption peak at around 440 nm. A theoretical study based on the use of the simulator COMSOL Multiphysics was developed. It was demonstrated, that the nanoparticles have a spheroids shape and their sizes are of the order of 12 nm. The theoretical results were validated by experimental results.

Keywords: *Silver nanoparticles, localized surface plasmon resonance, LSPR, modeling.*

M AMRAOUI
M REMRAM

LEMEAMED laboratory, Frères Mentouri University Constantine, Algeria.

1. INTRODUCTION

The silver nanoparticles are particularly attractive because of their single optical properties [1-3]. For example they exhibit a strong absorption band in the area UV-visible and an intense diffusion of the incidental light with scales length much smaller than the wavelength. It is the phenomenon of surface Plasmon resonance (SPR) [4-7] which occurs when the incidental light on the nanoparticles is in resonance with the collective oscillations of the electrons of conduction in metal nanostructures.

The metal nanoparticles are used in many applications such as chemical detections for example the detection of Mercury ions in aqueous mediums, biological detections for example the detection of bio markers or proteins sailing in the body fluids representative certain diseases cardiovascular and certain cancers, the imagery by the use of the nanoparticles like agent of contrast for the optical imagery, the delivery of therapeutic agent like drugs or genes and their release by external stimuli like the light and the thermal photo treatment targeted various diseases like cancer [8-14]. The plasmonic nanoparticles can be manufactured with a high degree of accuracy and in various forms [15] this with an aim of exploiting to the maximum their optical properties which extend from visible until the infrared, and which are influenced by the size and the form of the nanoparticles as well as dielectric medium surrounding them [16-18].This work concerns the synthesis of silver nanoparticles of controlled size. These nanoparticles are obtained by reduction of silver salt ($AgNO_3$) by the benzoic acid, in the presence of PVP .The size as well as the form of the nanoparticles are indirectly given according to the index of refraction of the solution of silver nanoparticles which we exploited in the study of three elaborate ideal models with software COMSOL Multiphysics based on the Finite Element Method (FEM) , in order to determine the nanoparticle which can qualitatively reproduce the behavior observed in experiments.

2. EXPERIMENTAL STUDY:

2.1 Materials:

The silver nitrate (Ag NO3,99.92% of purity) is used as precursor, the polyvinylpyrrolidone (PVP, the average molecular weight are of 40.000) is used like stabilizing, the benzoic acid is used like reducing agent, methanol and the ethanol is used as solvents.

2.2 Protocol of synthesis:

Silver nanoparticles were produced by a chemical process of reduction. A silver nitrate solution (0,0025 M of AgNO3) was prepared by diluting 0,42 g in 10 ml of ethanol with simultaneous mixture of a benzoic acid solution (0,5 G in 10 ml of ethanol) and the solution of PVP (1g in 10 ml of ethanol) to room temperature under vigorous magnetic agitation during 20 min. the mixture of reaction was heated at various temperatures (40 °, 50 °, 60 °, 70 °). Then, we varied the concentration of AgNO3 by taking the concentrations 0,0015M, 0.0030M, 0.0035M and by keeping same the other parameters.

The same protocol for the synthesis of the silver nanoparticles is remade with methanol.

2.3 UV-VISIBLE ABSORPTION SPECTROSCOPY

The study of the optical properties by spectroscopy of absorption constitutes one of the essential stages for the characterization of the silver nanoparticles synthesized.

It reveals the formation of silver nanoparticles thanks to the detection of a strong absorption of light by the nanoparticles in the area of the visible light.

The UV-visible spectra are recorded with a UV-visible spectrophotometer Ultrospec 2100 PRO, in a range wavelength extending from 200 to 900 nm.

Firstly we characterized our colloidal solutions according to the temperature for a concentration of AgNO3 of 0.0025

moles by holding the other constant parameters in two different solvents. The results obtained are gathered in the following table.

Table 1. Absorption maxima (λmax) of silver nanoparticles prepared from AgNO3 solution (0.0025 M) at different temperatures in different solvents.

AgNO3	λmax (nm)					
	30°	40°	50°	60°	65°	70°
In ethanol	446,1	439,8	444,1	445,1	_	439,6
In methanol	440,5	440,7	440,6	445,8	451,4	_

In the figure1, we present the absorption spectra for a concentration of AgNO3 of 0.0025 moles.

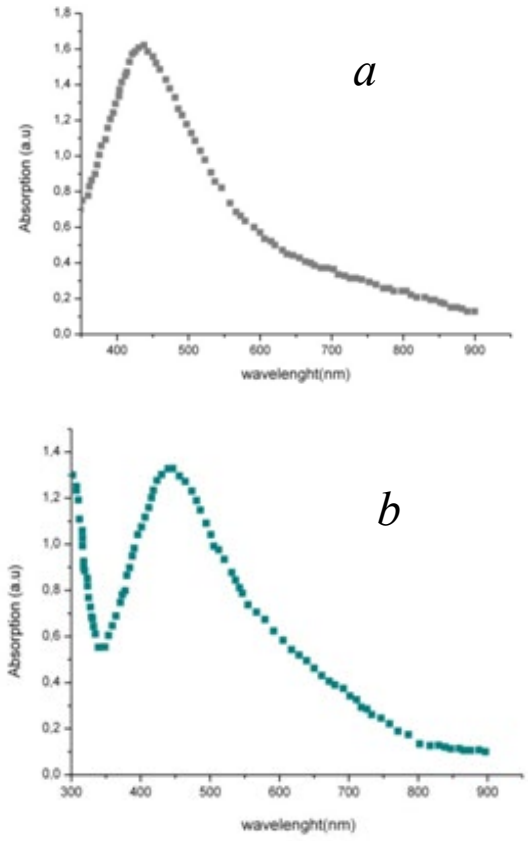

Fig1. UV-Vis absorption spectra of silver colloidal particles synthesized from AgNO3 solution (0.0025M) at 30°C in different solvents (a) Ethanol, (b) Methanol.

Then we varied the concentration of AgNO3 from 0.0015 to 0.0035 moles in two solvents, the samples are taken at constant temperature 30°.The results obtained are gathered on table 2.

Table2. Absorption maxima (λ_{max}) of the silver colloidal particles prepared from different concentrations of silver nitrate at room temperature 30° in different systems

AgNO3	λmax (nm)			
	0,0015 M	0,0025M	0,0030M	0,0035M
In ethanol	439,8	436,4	441,5	438
In methanol	435,6	440,5	446,2	442,4

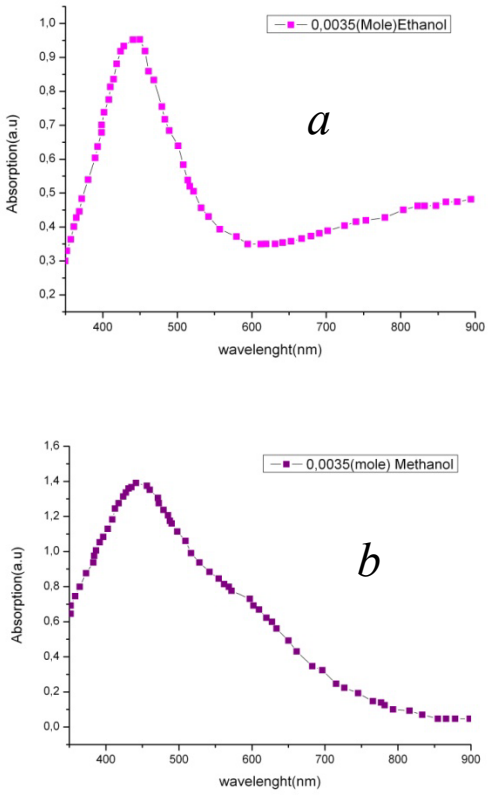

Fig2 .UV-vis absorption spectra of silver colloidal particles synthesized from $AgNO_3$ solution (0.0035M) at room temperature 30° in different solvents: (a) ethanol,(b)methanol.

Figure 2 presents an example of peak of absorption for the concentration 0.0035 mole.

We notice that the results obtained for ethanol are better contrary to the peaks of absorption obtained with methanol or we notice a spreading out of the spectrum, probably with a phenomenon of agglomeration of the silver nanoparticles

3. THEORETICAL STUDY:

3.1 *Ideal model:*

In order to predict the optical behavior of the nanoparticles worked out by chemical synthesis according to our preceding protocol, as well as the size and the form of the nanoparticles, we developed a theoretical approach while basing ourselves on the resolution of the Maxwell's

equations; by the finite element method, and while making use of simulator COMSOL Multiphysics.

One considers the electromagnetic-nanoparticle interaction wave described by the equation of wave of Maxwell [19]:

$$\nabla \times \left(\frac{1}{\mu_r}\nabla \times E\right) - k_0^2\left(\varepsilon_r - j\frac{\sigma}{\omega\varepsilon_0}\right)E = 0 \quad (1)$$

The absorption Coefficient Q_{abs} is obtained by integrating the thermal losses (U_{av}) compared to the volume of the nanoparticle:

$$Q_{abs} = \frac{1}{\pi r^2}\frac{2}{\sqrt{\varepsilon_0/\mu_0}E_{inc}^2}\int(U_{av})\,dV \quad (2)$$

Where E_{inc} is the amplitude of incidental electric field, r is the radius of the nanoparticle; ε_0 and μ_0 are respectively the permittivity and the permeability of the vacuum.

3.2 Results of modeling:

In first, we supposed that the nanoparticles worked out by chemical reduction have a form of nanospheres or nanorods or nanospheroids .The nanoparticles are surrounded by layers perfectly absorbing then excited by an electromagnetic wave wavelength of 400 nm - 800 nm parallel to polarize the major axis for the case of the spheroid and the stick. The experimental parameters used are: the permittivity of the silver nanoparticles which is extracted from the experimental data of Palik [20] and the index of refraction of the surrounding medium 1,34 and 1,37 which are respectively extracted from the colloidal solution with the solvent ethanol and methanol.

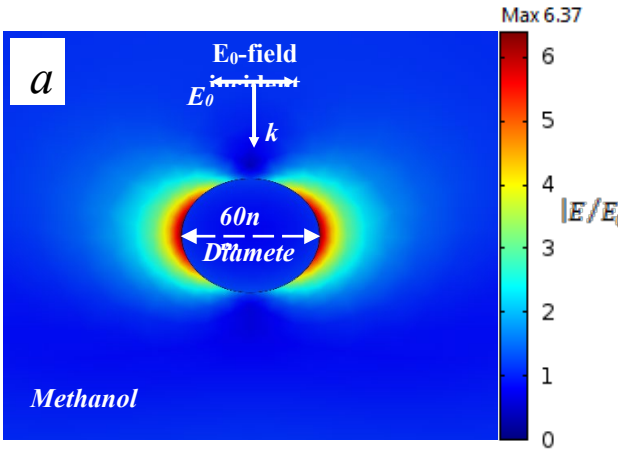

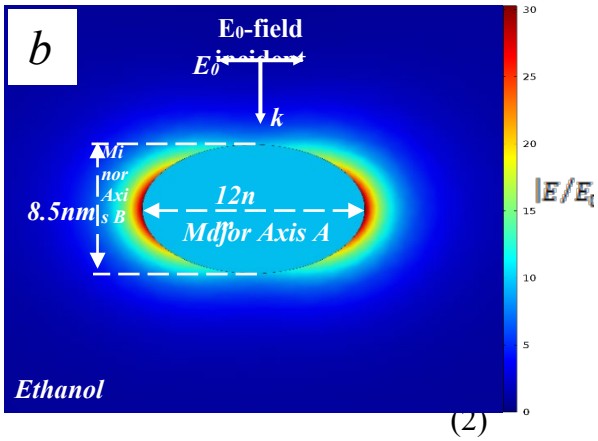

Fig 3: Contours of the electric field around: a) spherical and b) spheroid silver nanoparticles.

In the case of methanol we found for a wavelength similar to the experimental results, while basing ourselves on the theory of Mie, of the spherical nanoparticles, whose diameter is of 60 Nm; according to the spectra of the experimental results that it's rather an agglomeration of nanoparticles with certainly of irregular contours.

On the other hand for ethanol the results of the spheroids present exaltations of the fields to the wavelength obtained in experiments, and spectra similar between the two theoretical and experimental results from where any confirmation that the nanoparticles in a solvent ethanol have dimensions of 12 nm diameter and 1,4 nm of aspect ratio for a spheroid form. Nevertheless in a medium solvent methanol it is difficult to predict the form and the size of the nanoparticles because of the phenomenon of agglomeration.

4. CONCLUSION:

We proceeded to the study of the optical properties of the silver nanoparticles which are strongly influenced by the size, the form, the index of refraction of the surrounding medium but also by the physical and chemical experimental conditions. The UV-visible absorption spectroscopy of the solutions of silver nanoparticles prepared for various molar concentrations of AgNO3 with various temperatures in various systems shows for the majority of them only one peak of absorption. However the temperature probably acts on the widening of the absorption spectra of the nanoparticles resulting from methanol medium due to a phenomenon of agglomeration. The results of simulation by software COMSOL Multiphysics show an agreement of the silver nanoparticles synthesized in solvent ethanol with the spheroid model of 12 nm diameter. On the other hand, it is difficult to predict the form and the size of the nanoparticles in a medium solvent methanol because of the phenomenon of segmentation.

REFERENCES

[1] Mohamed MB, Volkov V, Link S, Sayed MAE (2000) The 'lightning' gold nanorods: fluorescence enhancement of over a million compared to the gold metal. Chem Phy Lett 317:517–523

[2] Mounira Amraoui, Chouaib Daoudi, Mohamed Remram "Preparation and Characterization of Silver Nanospheroids: Theoretical and Experimental Approaches". PHOTONICS LETTERS OF POLAND, VOL. 9 (2),63-65 (2017)

[3] Chouaib Daoudi, Mahmoud Ould Metidji, Mohamed Remram, Anne-Marie Jurdyc, Matteo Martini, Hélène Gehan and Dominique Vouagner "Nano-assembling and optical properties of sub-100 nm raspberry-like nanoparticles" Eur. Phys. J. Appl. Phys. 82, 20401 (2018).

[4] Xiaohua Huang, Mostafa A. El-Sayed, *journal of advenced research*, 1, 13-28 (2010)

[5] Xiu-yu Liu, Cong-ying Cui, Ying-wen Cheng, Hou-yi Ma and Duo Liu, *International Journal of Minerals, Metallurgy and Materials*, 20 (5), 486–492 (2013)

[6] C.F. Bohren, D.R. Huffman, Absorption and Scattering by Small Particles, Wiley-Interscience, New York, 1983.

[7] U. Kreibig, M. Vollmer, Optical Properties of Metal Clusters, Springer, Berlin, 1995.

[8] .J-S Lee, MS Han, CA Mirkin. Angew. Chem. 119(22), 4171–4174 (2007).

[9] Eleonora Petryayeva, Ulrich J. Krull.A reviewAnalytica Chimica Acta 706 (2011) 8– 24

[10] Elodie Boisselier and Didier .Chem. Soc. Rev., 2009, 38, 1759–1782

[11]. J Chen, F Saeki, BJ Wiley, H Cang, MJ Cobb, Z-Y Li, L Au, H Zhang, MB Kimmey, Li, Y Xia,. Nano Lett. 5(3), 473–477 (2005)

[12]. EB Dickerson, EC Dreaden, X Huang, IH El-Sayed, H Chu, S Pushpanketh, JF McDonald, MA El-Sayed. Cancer Lett. 269(1), 57–66 (2008)

[13]. KY Lin, AF Bagley, AY Zhang, DL Karl, SS Yoon, SN Bhatia. Nano LIFE 1(3), 277–287 (2010)

[14] P.K. Jain, X. Huang, I.H. El-Sayed, M.A. El-Sayed, Acc. Chem. Res. 41 (2008)1578.

[15] Nikolai G. Khlebtsov, lev A.Dykman, *journal of quantitative spectroscopy and radiative transfer*, 111, 1-35 (2010)

[16] Kelly, K. L., Coronado, E., et al, Journal of Physical Chemistry B 107(3): 668-677 (2003).

[17] Link, S. and El-Sayed, M. A. Journal of Physical Chemistry B103 (21) (1999).

[18] Min Hu,ae Jingyi Chen,a Zhi-Yuan Li,b Leslie Au,a Gregory V. Hartland,c Xingde Li,d Manuel Marqueze and Younan Xia,Chem. Soc. Rev., 2006, 35, 1084–1094 (2006)

[19] J.C Maxwell Garnett, Phil.trans.R.Soc.Lond.A,vol.203,no.359-371,pp.385-420 ,1904.

[20] E.D.Palik.Academic Press Inc (1985).

FATIGUE LIFE PREDICTION OF UPPER ARM SUSPENSION USING STRAIN LIFE APPROACH.

Submitted on 18/03/2018 – Accepted on 23/12/2018

Abstract

This paper presents the fatigue life behavior of upper arm suspension under cyclic loading. The main objectives are to predict the fatigue life of the component using strain life approach, to identify the critical location and to select the suitable materials for the suspension arm.To conduct this analysis three aluminum alloys were selected for the suspension arm, to do so CAD model of upper arm is designed in Solid Works and imported in a finite element ANSYS code. The upper arm was subjected to constant amplitude loading in z direction and boundary conditions were applied at the end of bushing. Tetrahedral elements gives enhanced results as compared to other types of elements, therefore the elements used in this analysis is (TET 10); the maximum principal stress is considered in the linear static stress analysis and the critical location was considered at node 63754.The finite element model and analysis were performed utilizing the finite element analysis code. Finally, damage is evaluated to the remaining capacity of life and then the stress and strain at the critical region are estimated. From the fatigue analysis Aluminum alloys 7175-T73 and 2014-T6 presents a similar behavior compared to 6061-T6 , in this case of study these lather are considered to be the materials of choice to manufacture the suspension arms; but 7175-T73 Aluminum alloys remains the material with a better resistance to fatigue.

Keywords: *Upper Suspension arm, finite element analysis, constant amplitude loading, strain-life method, critical location.*

H KAHOUL [1]
S BELHOUR [1]
A BELLAOUAR [2]

1 Mechanical engineering department, Frères Mentouri University Constantine, Algeria.

2 Transportation engineering department, Frères Mentouri University Constantine, Algeria.

I. INTRODUCTION

The suspension system is one of the most important components of vehicle, which directly affects the safety, performance, noise level and style of it. The vehicle suspension system is responsible for driving comfort and safety as the suspension carries the vehicle-body and transmits all forces between body and road **[1]**. In the automotive industry, the riding comfort and handling qualities of an automobile are greatly affected by the suspension system, in which the suspended portion of the vehicle is attached to the wheels by elastic members in order to cushion the impact of road irregularities. Suspension arm is one of the main components in the suspension systems; it joins the wheel hub to the vehicle frame allowing for a full range of motion while maintaining proper suspension alignment. Uneven tire wear, suspension noise or misalignment, vibrations are the main causes of the failure of the lower suspension arm. Most of the cases the failures are catastrophic in nature as the Finite element method (FEM) gives better visualization of this kind of the failures so FEM analysis of the stress distributions around typical failure initiations sites is essential. Therefore in this paper it is proposed to carry out fatigue analysis of upper suspension arm of light commercial vehicle using FEM.

Fatigue analyses can be performed using either one of the three basic methodologies including the stress-life approach, strain-life approach **[2]** and crack growth approach. The stress-life method was first applied over a hundred years ago and considers nominal elastic stresses and how they are related to life. This approach to the fatigue analysis of components works well for situations in which only elastic stresses and strains are present however, most components may appear to have nominally cyclic elastic stresses but stress concentrations present in the component may result in local cyclic plastic deformation. Under these conditions, fatigue analysis using the local strain-life method uses the local strains as the governing fatigue parameter and capable of handling significant levels of cyclic plasticity **[3].**

The strain-life approach can be used proactively for a component during early design stages and the fatigue resistance of metals can be characterized by a strain-life curve see Fig1. The relationship between the total strain amplitude ($\Delta\varepsilon/2$) and the reversals to failure (2Nf) can be expressed in Eq. (1) **[4-5].**

$$\frac{\Delta\varepsilon}{2} = \frac{\sigma_f}{E}(2N_f)^b + \epsilon_f(2N_f)^c \qquad (1)$$

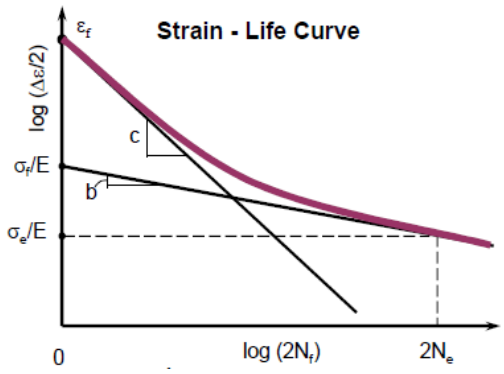

Fig 1. Strain life curve **[6].**

Where N_f is the fatigue life, σ_f is the fatigue strength, E is the modulus of elasticity, b is the fatigue strength exponent, ε_f is the fatigue ductility coefficient, and c is the fatigue ductility exponent. It should be noted that this methodology is based on the fact that plastic deformation is a small fraction of total deformation; this is why this method delivers good estimates in high fatigue cycle regions where elastic deformation controls the processes of fatigue damage. So, this methodology is not unique as a tool for low cycle and high fatigue cycle prediction **[7].** The local strain-life approach is preferred if the loading history is irregular and where the mean stress and the load sequence effects are thought to be of importance. The strain-life approach involves the techniques for converting the loading history, geometry and materials properties (monotonic and cyclic) input into a fatigue life prediction. First, the stress and strain at the critical region are estimated then, the crack initiation methods are employed to predict the fatigue life. The simple linear hypothesis proposed by Palmgren **[8]** and Miner **[9]** is used to accumulate the fatigue damage. Finally, the damage values for all cycles are summed until a critical damage sum (failure criteria) is reached. The concept of damage represents the state of degradation of the material considered. This state result in a quantitative representation of the endurance of the materials subjected to various loading history; a cumulative damage law is, for its part, a rule for accumulating damage variable D as for the service life; it is defined by a number of cycles N which leads to the rupture thus, the application of n cycles (n <N) causes a partial deterioration of the part considered for the calculation. The evaluation of the damage, at a given moment, is decisive to evaluate the remaining capacity of life. Fatemi and Yang **[10]** have documented in the literature more than fifty laws of cumulative damage; the most used today is that of linear damage Palmgren-Miner remains the best compromise between the simplicity of application and the quality of forecasts for long life **[11].** The Miner's rule is as follows:

$$d_i = \frac{n_i}{N_I} \qquad (2)$$

With n_i number of repetitions of a given cycle (with amplitude or range), N_i number of repetitions of the same cycle required to declare the failing component ($n_i < N_i$). For the different cycles of the random solicitation studied, the overall damage is obtained by linear addition of the elementary damages:

$$D = \sum_i d_i = \sum_i \frac{n_i}{N_i} \qquad (3)$$

2. MATERIAL INFORMATION :

Material model and material properties play an important role in the result of the FEM. The material properties are one of the major inputs which is the definition of how a material behaves under the cyclic loading conditions. The cyclic material properties are used to calculate the elastic-plastic stress-strain response and the rate at which fatigue damage accumulate due to each fatigue cycle. The materials parameters required depend on the analysis methodology being used. The mechanical properties of Materials used in this analysis are shown in Table 1.

Table 1: **Materials properties of Aluminum alloys**

	Aluminum alloy 2014-T6_125_HF	Aluminum alloy 6061-T6_80_HF	Alumin alloy 71 T73_NON
Tensile strength, σ_{UTS} (MPa)	483	340	524
Yield strength, σ_{YS} (MPa)	437	313	447
Young's modulus, E (GPa)	72.7	72.7	71.3
Fatigue strength exponent, b	-0.12	-0,097	-0.082
Fatigue strength , σ_f (MPa)	976	645	765
Fatigue ductility exponent, c	-0.88	-0.6	-1.14
Fatigue ductility coefficient, ε_f	0.88	0.22	6.18

3. MODEL DESCRIPTION

Vehicle suspension is a mechanism locating between the sprung mass (vehicle body) and the unsprung masses (wheels) of the vehicle. The suspension provides forces between these two masses of the vehicle according to certain state variables of the vehicle. A good car suspension system should have satisfactory road holding ability, while still providing comfort when riding over bumps and holes in the road. A simple three-dimensional model of suspension arm was modeling by using Solid Works software then imported to Ansys finite element code. Fig 2. shows the structural model **[12].**The weight is 1.19 kg and the size is 320mm x 260mm x 68mm **[13, 14 and 15].**

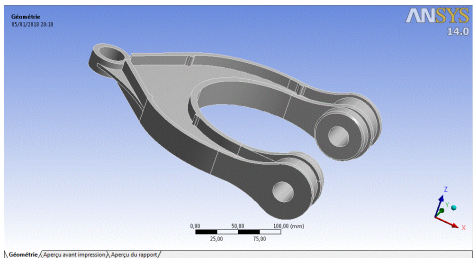

Fig 2. Three-dimensional FE model

4. MESH GENERATION :

In this analysis mesh generation is auto generation by the ANSYS software, after that sizing of 3mm was given to the suspension arm. Tetrahedral 10-noded elements were used to mesh the upper suspension arm, see Fig 3.

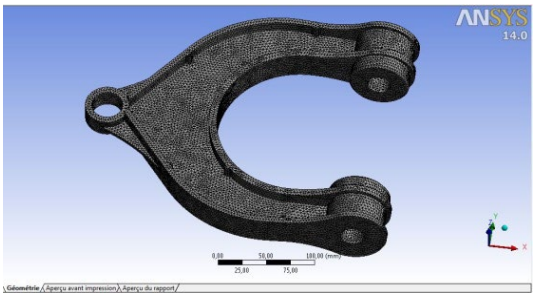

Fig 3. Mesh model with tetrahedral element (TET 10)

5. LOADING

We consider vertical force 2500 N is loaded with constant amplitude in Z direction **[16]** applied at the end of the bushing that connected to the tire. The other two bushing that connected to the body of the car are constraint. The three-dimensional FE model, loading and constraints of suspension arm is shown see Fig4**. [17].**

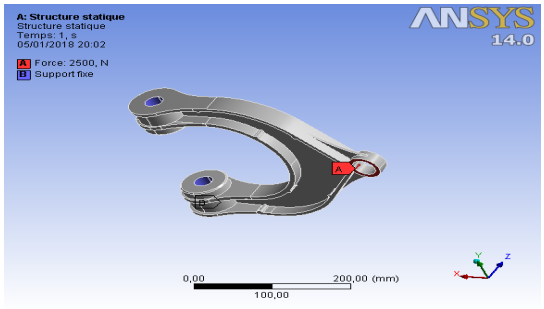

Fig 4. Boundary conditions and force loading

Loading is of constant amplitude because only 1 set of finite element stress results along with a loading ratio is required to calculate the alternating and mean stress. The loading ratio is defined as the ratio of the second load to the first load

$$R = {}^{\sigma_{min}}/_{\sigma_{max}} \qquad (4)$$

In this study constant amplitude loading is fully reversed (apply a load then apply an equal and opposite load; a load ratio of -1).

5. RESULTS AND DISCUSSION

In this analysis we use Ansys software based on (FEM), it is known for its high performance, quality and ability to solve all kinds of challenging simulations.

Aluminum alloys

6061-T6

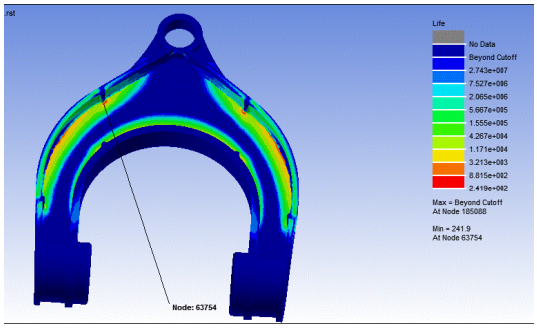

zoom at critical node

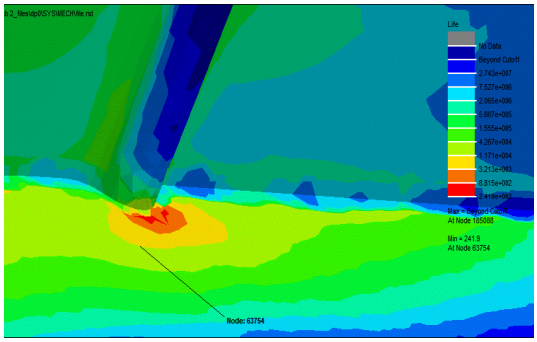

2014-T6

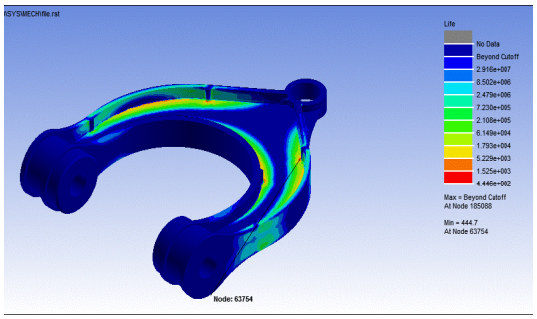

7175-T7

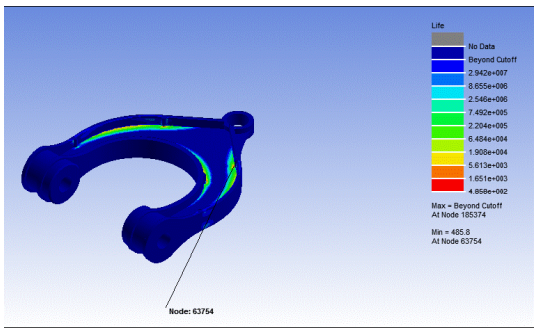

Fig 5. Predicted life contour .

Fig 5. shows predicted life contour plotted for the three aluminum alloys; we see that 6061-T6 aluminum alloys presents the shortest life at node 63754.

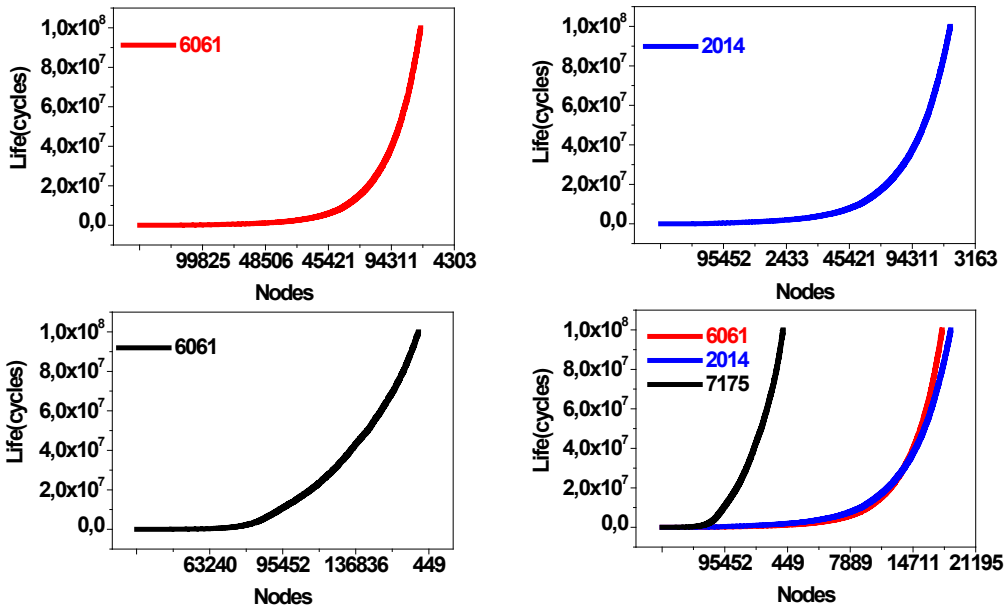

a) At all nodes

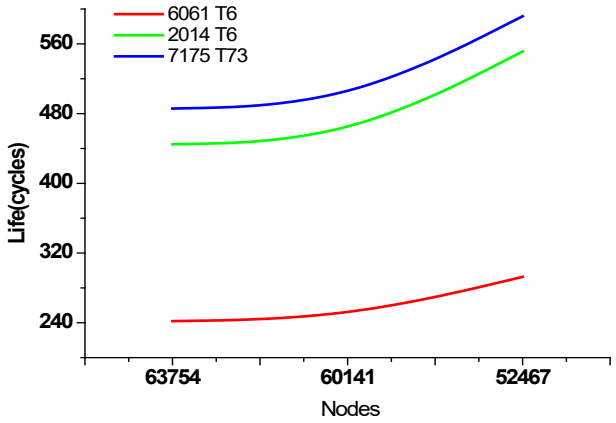

b) At 10 hot spot nodes

Fig 6. Composite plot for three materials Predicted life-nodes curves.

Fig 6. shows the increase of life a) at all nodes and , b) at 10 hot spot nodes. We see clearly that the critical area is at node 63754. Among the three studied materials, 6061-T6 shows the shortest fatigue life (241.9 cycles) due to the development of stress concentration near singularitie which led of a large deformation.

Fig 7. shows damage contour plotted for the same materials ; the higher damage corresponds to 6061-T6 aluminum alloy since it has the shortest life.

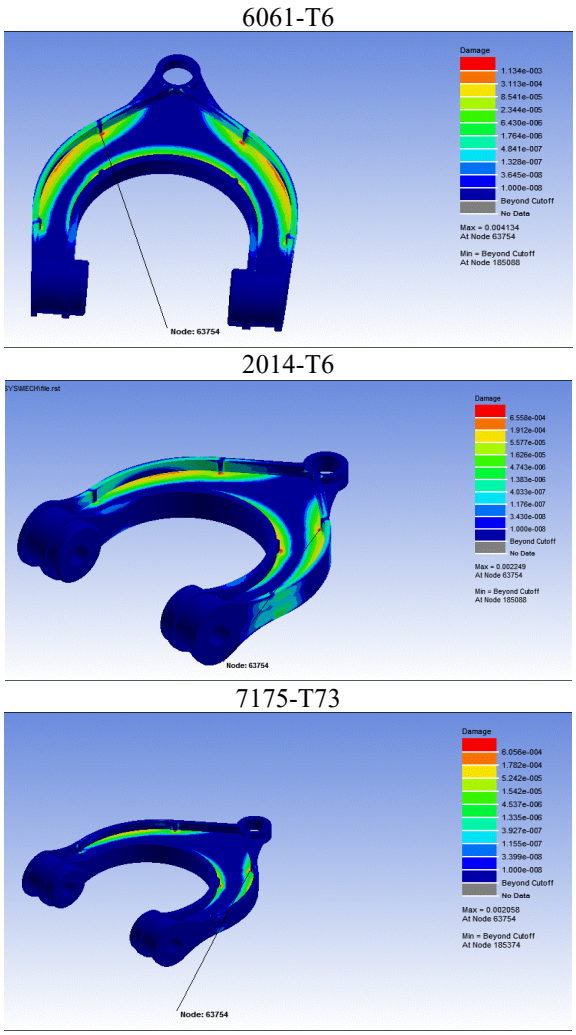

Fig 7. Damage contour plotted.

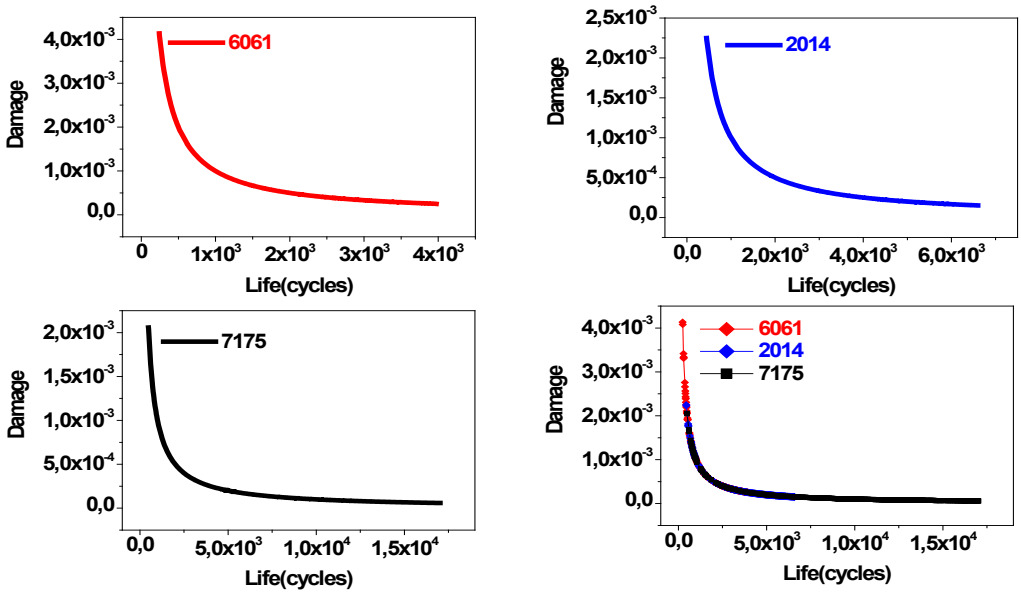

a) At all nodes

b) At 10 hot spot nodes

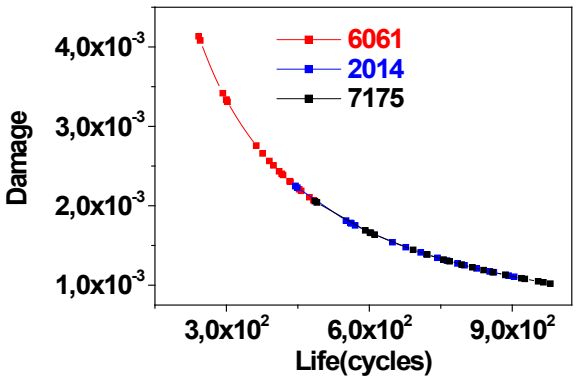

Fig 8. Composite plot of three materials Damage-Life curves

Fig 8. shows damage according to the number of cycles which decreases with increasing cycles.We note that for cycles less than 500 cycles the damage is more important. The higher damage of 4.13 E-3 at node 63754 corresponding to 241 cycles is that of 6061-T6. The damage depends on strain rate. For life less than 500 cycles the deformation is mainly plastic,whereas for life larger than 500 cycles the deformation is mainly elastic.

Fig. 9 shows strain contour plotted for the three aluminum alloys ; we see clearly that the maximum strain observed at node 63754 is for 6061-T6.

6061-T6

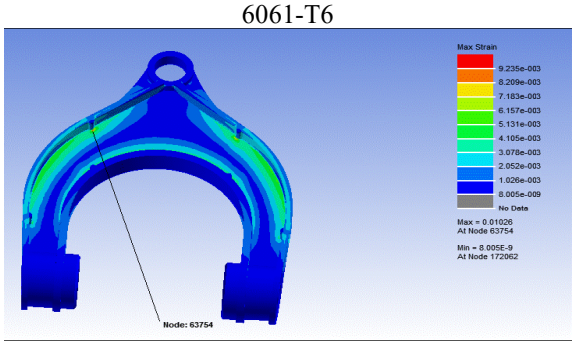

2014-T6

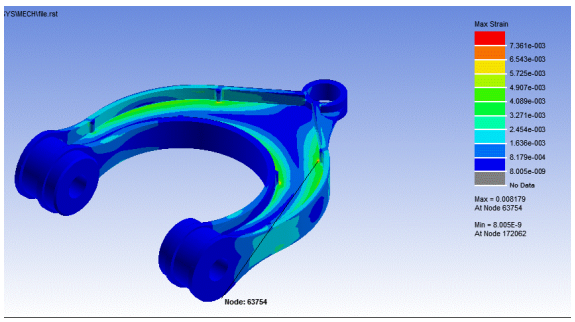

7175-T73

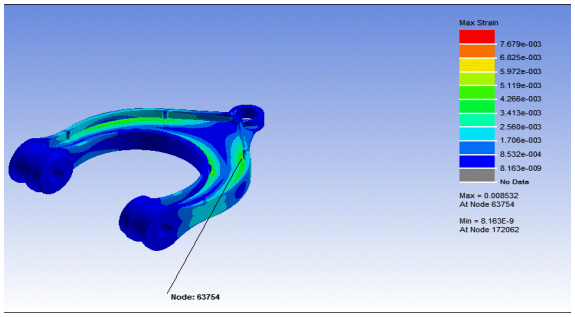

Fig 9. Strain contour plotted

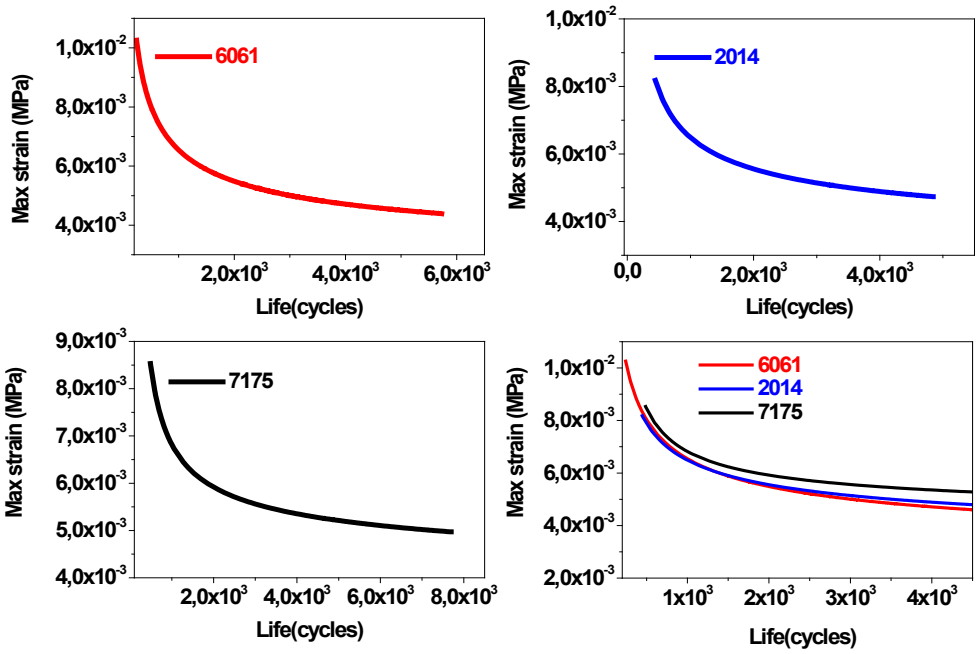

a) at all nodes

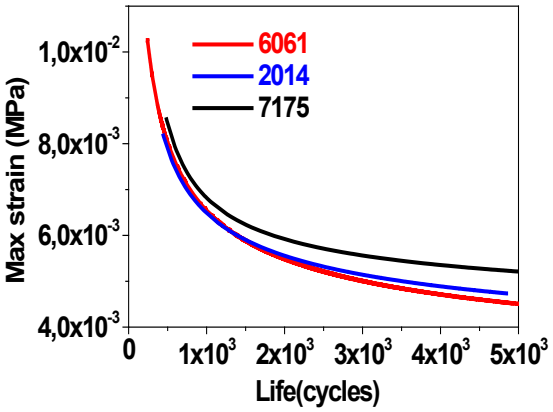

b) at 10 hot spot nodes

Fig 10. Composite plot of three materials Stress-Life curves

Fig 10. presents graph of strain according to the number of cycles; this graph shows that the strain decrease when the predicted life increases; the max strain observed for 6061-T6 is 10.26 E-3 at critical node which correspond to a minimum life of 241.9 cycles.

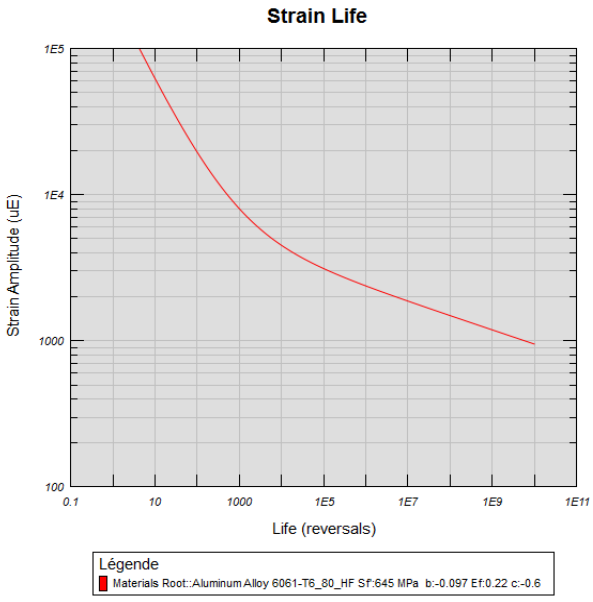

a) 6061

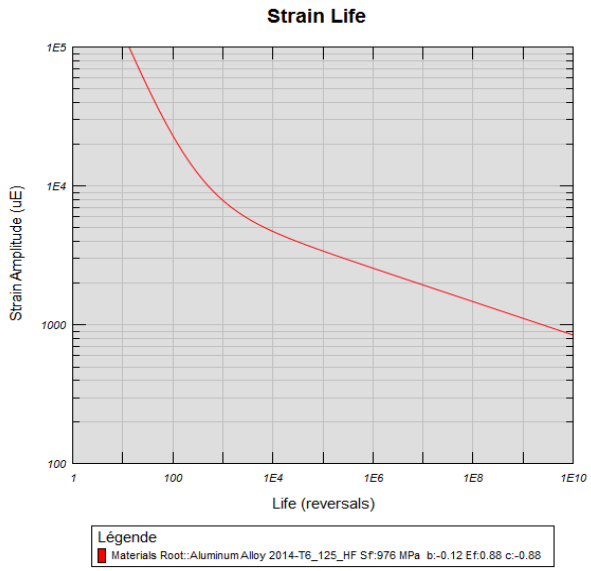

b) 2014

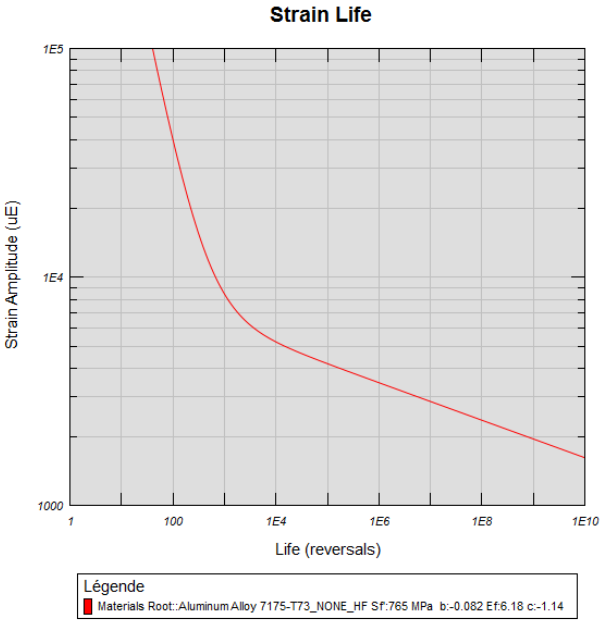

c) 7175

Fig 11. Strain amplitude vs life [2].

Fig 11. shows results tests carried out on three aluminum alloys ; it is clear that the material with the shortest life is 6061-T6 which confirms the appearance of the curves drawn in Fig.10 from the simulation.

6061-T6

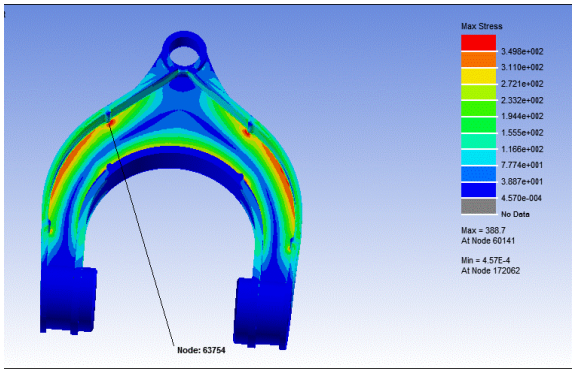

2014-T6

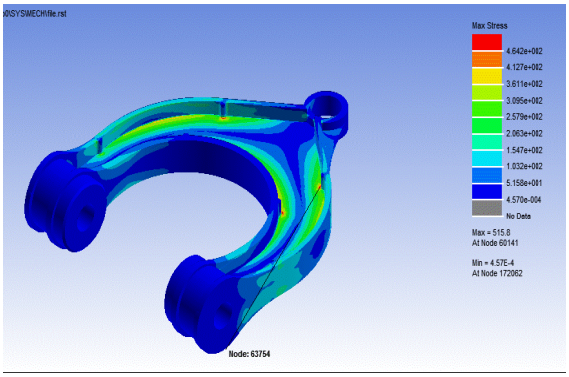

7175-T73

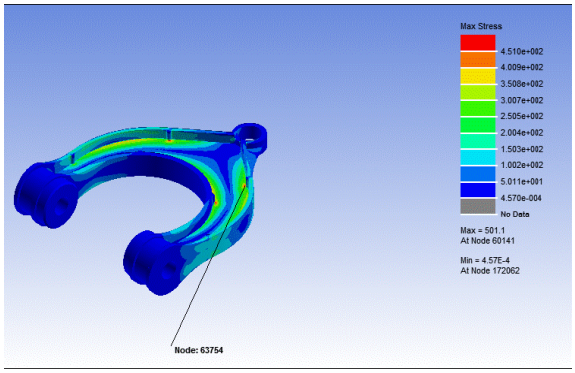

Fig 12. Stress contour plotted.

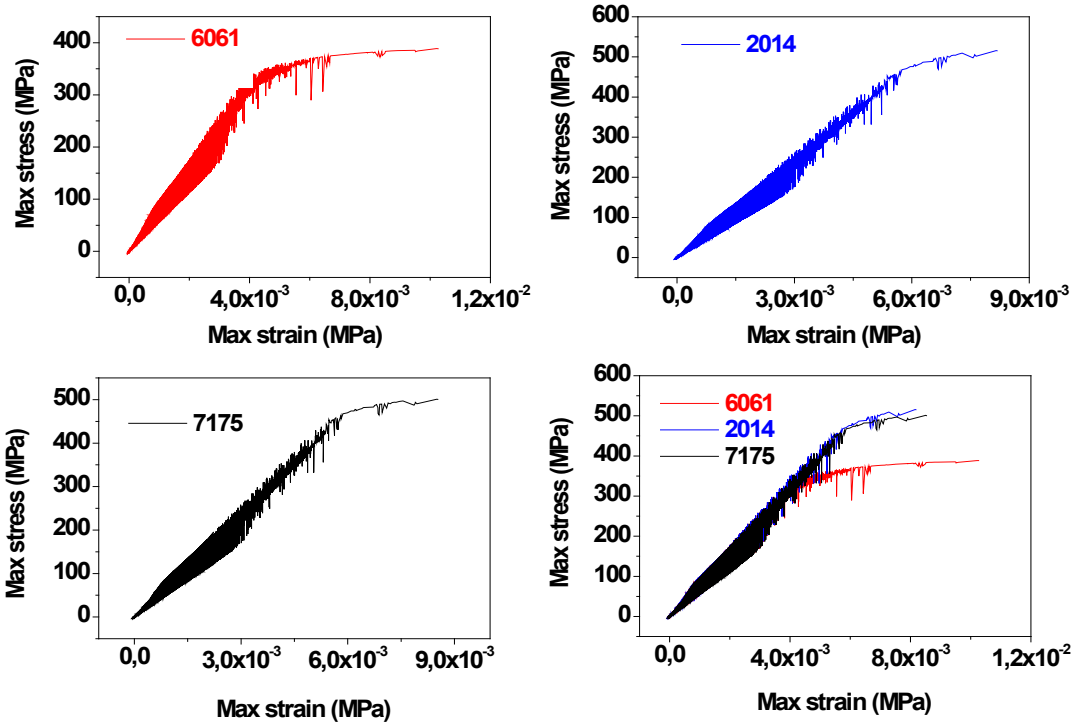

Fig13. Stress amplitude vs. Strain amplitude

Fig 12. shows stress contour plotted for the three materials however Fig 13. shows the evolution of stress according to deformation, we note that for the same loading the levels of constraints and deformations reached for the three materials are not the same, with small difference for 7175 and 2014; however the largest deformation reached is that of 6061 (10.26 E-3) at the critical node 63754 it corresponds to the smallest constraint (388.6 MPa).We also note that the stress levels reached at critical node for three materials exceed their tensile strength which results in elastoplastic behavior of the latter.

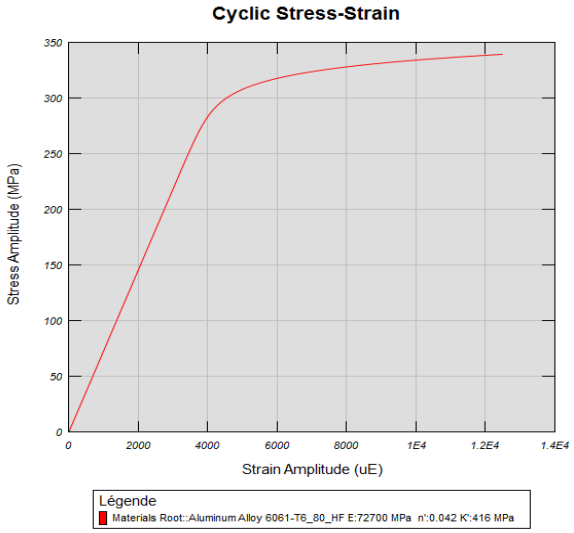

a) 6061

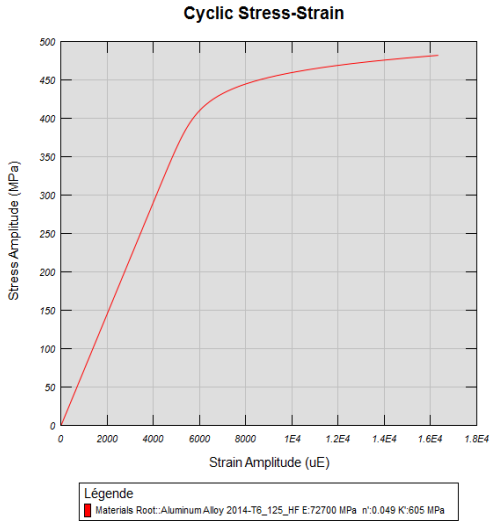

b) 2014

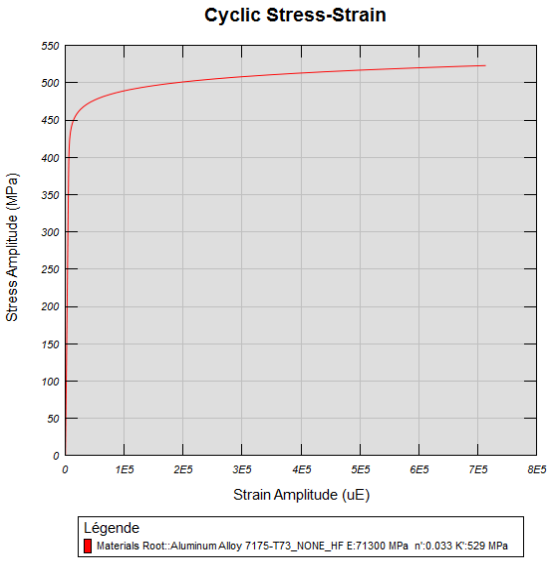

c) 7175

Fig14. Tests stress vs. strain for three materials [2].

Fig 14. shows the stress-strain tests results obtained for the three materials it is clear that there is a correlation between these graphs and the results obtained by simulation. The table 2 summarize the results of the fatigue analysis of the upper arm suspension.

Table 2 Fatigue analysis results for the three materials

	Life cycles	Damage	Max stress MPa	Max strain
6061-T6_80_HF	241.9	4.13 E-3	388,6	10.26 E-3
2014-T6_125_HF	444.7	2.24 E-3	515.8	8.17 E-3
7175-T73_NONE_HF	485.8	2.05 E-3	501.1	8.53 E-3

Table 2. shows the results obtained from a fatigue life analysis conducted for three aluminum alloys with different mechanical properties. For 7175-T73 and 2014-T6, the stress values gives almost similar deformations as well as the resulting damage, which explains the similarity of the behavior. The maximum stresses obtained are 515.8 MPa and 501.1 MPa respectively exceeding their tensile strength σ_{UTS} (483 MPa and 524 MPa) ,where the deformations values are of the order of 8.17 E-3 and 8.53 E-3 at node 63754, we can notice that for approximatively the same range of stress gives the same life and strain . We can also see that the damage caused in the first material (2014-T6_125_HF) is slightly higher than in the second one (7175-T73_NONE_HF), a large deformation led to a small damage against a small deformation led to a great damage. However for 6061-T6 for the same loading the level of stress is the smallest with a value of (388.6 MPa), as well as the deformation is (10.26 E-3) and damage rate is the greatest one (4.13 E-3).

6. CONCLUSION

In this study a strain-life approach based on finite element of the fatigue life prediction of a upper arm suspension is presented. The calculation is carried out using Ansys nCode Design Life, one of the leading commercial durability software tools worldwide .Three materials were used to conduct this analysis. Hot spot detection is used to identify the critical areas of the model, 10 most damaged areas are identified, highlighting the worst node in each area. The result of the fatigue analysis based on strain life approch is a life and damage contours plotted for three aluminum alloys, life and damage values are calculated for every node and the red color indicates the minimum life and the maximum damage at critical areas in the component . We see clearly the decrease in life when damage increase. Also the maximum values of stress and strain in each node are évaluated. Finally the fatigue life analysis is focused on node 63754 where there is a local accent constraint near a singularity. This study highlight the influence of the singularities on the behavior of the upper arm. The comparison of the fatigue behavior for the three materials showed the similarity of the behavior between 2014 and 7175 because their fatigue lifes are close as well as the deformations resulting. However for 6061 the deformation obtained is greater which led to a smaller life of around 50% compared to the two others.

This study shows that 7175-T73 and 2014-T6 aluminum alloys suspension arm presents a better resistance to fatigue and higher life compared to 6061-T6 aluminum alloys. Thus, these lather are considered to be the materials of choice in this case of study.this comparison allows us to made it possible to understand their performances and the mechanisms of damage within the suspension arm as well as the values of the fatigue life obtained.

From this study we could notice that:

- At large strains or short lives, the plastic strain component is predominant, and at small strains or longer lives the elastic strain component is predominant.
- At larger strains, increased life is dependent more on ductility, while at smaller strains longer life is obtained from higher strength materials.
- Most fatigue failures begin at local discontinuities where local plasticity exists and crack nucleation and growth are governed by local plasticity at the notch tip.
- The optimum overall strain-life behavior is for tough metals, which are materials with good combinations of strength and ductility larger strains.

REFERENCES

[1]. Shaikh Ateekh Abdul Naeem, P. V. Jagtap. Analysis of Upper Control Arm for finding optimized model using FEA and Experimentation. Imperial Journal of Interdisciplinary Research (IJIR) Vol-3, Issue-3, 2017.

[2]. M. M. Rahman,K. Kadirgama,M. M. Noor,M. R. M. Rejab,S. A. Kesulai. "Fatigue Life Prediction of lower suspension arm using strain-life approach". European journal of scientific research Vol.30 No.3 (2009), pp.437-450.

[3]. NCode Design Life User Guide, HBM United Kingdom Limited 2012.

[4]. Morrow, J. 1968. Fatigue Design Handbook: Advances in Engineering. Warendale, PA: SAE, 21-29.

[5]. Smith, K.N., Watson, P. and Topper, T.H. 1970. A stress-strain functions for the fatigue on materials. Journal of Materials. 5 (4): 767-78.

[6].*https://www.efatigue.com/training/Strain_Life_Method.pdf.*

[7]. Abdel Hamid Saoudi, "Prédiction de la rupture par fatigue dans les pièces automobiles en alliages aluminium" .Thèse de doctorat, 2008, Université du Québec à Chicoutimi.

[8]. Palmgren, A., 1924. Durability of ball bearings. ZVDI, 68(14): 339-341.M.

[9]. Miner, A., 1945. Cumulative damage in fatigue. Journal of Applied Mechanics. 12: 159-164.

[10]. Fatemi (A.) et Yang (L.). – Cumulative fatigue damage and life prediction theories : a survey of the state of the art for homogeneous materials. Int J Fatigue, 20(1), p. 9-34 (1998).

[11]. BANVILLET (A.). "Prévision de durée de vie en fatigue multiaxiale sous chargements réels : vers des essais accélérés". Thèse de doctorat N° 2001-17 (274 p.), ENSAM Bordeaux,France (2001).

[12]. Journal of Advanced Science and Engineering Research 1 (2011) 42-52.

[13]. T. Lindby and J.L.T. Santos; Shape optimization of three-dimensional shell structures with the shape parameterization of a CAD system, (1999), Page 6.2.

[14]. J. E. Shigley, C. R. Mischke, McGraw Hill; Mechanical Engineering Design, 6 edition, (2000).

[15]. Paul Haney; Basic Vehicle Dynamics, (1999), Page 22.

[16]. Jagwinder Singh, Siddhartha Saha . "Static structural analysis of suspension arm using finite element method": IJRET-International Journal of Research in Engineering and Technology eISSN: 2319-1163 | pISSN: 2321-7308.

[17]. Savan Thacker1 and Antriksh Bhatt2. "Design and Analysis Double Wishbone Suspension System using Finite Element Analysis". IJSRD - International Journal for Scientific Research & Development| Vol. 2, Issue 09, 2014 | ISSN (online): 2321-0613.

CHOICE OF THE PRIOR IN THE BAYESIAN DESIGN FOR THE CLINICAL TRIALS.

Submitted on 12/04/2016 – Accepted on 24/10/2016

Abstract

Bayesian statistics have the advantage of being easily established and derived. Thus, we will use this approach to find the distribution of the predictive probabilities of the data not observed yet in the conception of clinical trials phase II. Such perspectives are necessary in cases or in reason treat ethical preoccupations or ether to achieve trials which are particularly toxic or expensive. We propose, in reason of neutrality, to calculate the predictive probabilities within a Bayesian case, where the prior is non informative in different models apply in clinical trials.

Keywords: *Bayesian prediction, p-value, clinical trials, non informative prior.*

ZOHRA DJERIDI [1]
HAYET MERABET[2]

1 Mathematics Department, Jijel University, Jijel, Algeria;

2 Mathematics Department, Laboratory of Applied Mathematics and Modeling, Constantine1 University, Algeria.

I- Introduction

Clinical trials are prospective studies to evaluate the effect of interventions in humans under prespecified conditions. They have become a standard and integral part of modern medicine. A properly planned and executed clinical trial is the most definitive tool for evaluating the effect and applicability of new treatment modalities ([3]; [4]; [5]; [7]). The methodology adapted to the context of clinical trials is characterized by many constraints and unsatisfactions and form the subject of a deep and continuous development ([1]; [5]; [6]; [8). One of the reasons of such interest likely holds from the fact that public health authorities are responsible for the authorization of putting the drugs into market and they play a primordial role in the elaboration of rigorous methodology of clinical trials in the view of all the actors in this field (industries, public institutes of research, hospitals and scientific journals).

The clinical trials primary goal is to evaluate the efficiency and the tolerance of a new medical treatment, they are characterized by complex actions that can't be readily modeled and they do not depend solely on statistical considerations (see for example Shein-Chung Chow, and al., [2]).

The Bayesian approach brings a major flexibility to the statistic methodology of the clinical trials. In particular we are interested to use this approach in prediction in the context of clinical trials because of the critical role which play the predictive probability in the design of a trial and also in monitoring trials. In this situation, often we have got primary experimental information in the form of phase I which we need to confirm some results ([2], [8]). Formally, we consider the following situation: To go by the data of the first sample, we can plan an experience (a new sample) so as to have good chances to get the intended conclusion if the experimentation is not discarded. We propose the procedure based on the concept of the index of satisfaction which is a function of the *p-value*, and we envisage, given the available data, to calculate a predicted satisfaction of this index conditioning to the previous observations ([8]). To illustrate this procedure, we will study several exponential models chosen a non-informative prior to make evidence to the analysis objectivity of the experimental data. The numeric calculations and the simulation results are presented in the form of Gaussian model.

2. Statistic method :

We recall (see Merabet [8]), that the experimental context consists of two successive experimentations, of results $\omega' \in \Omega'$ and $\omega'' \in \Omega''$, which are in general carried out independently. Their distributions built in the framework of a well established model, depend on a parameter $\theta \in \Theta$, only $\omega"$ is used to found the official conclusion of the study and to determine the user satisfaction denoted $\phi(\omega")$ (and on the choice about which we will come back in 3). But, on the basis of the result ω' of first step clinical trial, it is useful to anticipate what the satisfaction will be well after the second step. In our study, this prediction is carried out in a bayesian context, i.e., based on the choice of a prior probability on Θ. We therefore define the indicator of prediction as:

$$\pi(\omega') = \int_{\Omega''} \phi(\omega") P_{\Omega''}^{\omega'}(\omega'') \qquad (1)$$

Where $P_{\Omega''}^{\omega'}(\omega'')$ is the probability on Ω'', conditioned by the result of the first step, and $\phi(\omega")$ is the index of satisfaction, given also as:

$$\pi(\omega') = \int_{\theta} \left(\int_{\Omega''} \phi(\omega") P_{\Omega''}^{\theta}(\omega'') \right) P_{\theta}^{\omega'}(\theta) \qquad (2)$$

Were $P^{\theta}_{\Omega''}(\omega'')$ is the sampling distribution of the second step, and $P^{\omega'}_{\Theta}(\theta)$ is the posterior probability on Θ, based on the result of the first step. Let us consider the case where one has densities relative with measurements μ, ν' and ν'' on Θ, Ω' and Ω'', that of the prior P_Θ being denoted g and those of the sampling probabilities $P^{\theta}_{\Omega'}$ and $P^{\theta}_{\Omega''}$ being denoted $f'(.|\theta)$ and $f''(.|\theta)$ respectively. (1) and (2) then become:

$$\pi(\omega') \frac{\int_{\Omega''} \phi(\omega'') \left(\int_{\Theta} f'(\omega'|\theta) f''(\omega''|\theta) g(\theta) \mu(d\theta) \right) \nu''(d\omega'')}{\int_{\Theta} f'(\omega'|\theta) g(\theta)\, \mu(d\theta)} \quad (3)$$

And

$$\pi(\omega') = \frac{\int_{\Theta} \left(\int_{\Omega''} \phi(\omega'') f''(\omega''|\theta) \nu''(d\omega'') \right) f'(\omega'|\theta) g(\theta) \mu(d\theta)}{\int_{\Theta} f'(\omega'|\theta) g(\theta)\, \mu(d\theta)} \quad (4)$$

2.1. Index of satisfaction

This concept is important when the statistician, who carries out a test, "wishes" to observe a significant result, that is to reject the null hypothesis H_0. Its satisfaction will be thus larger in the event of rejection, and even in general as much larger as the observation that leads to this rejection is more significant. It's what even the users put in an obvious place, at the end of a test, not only the conclusion "all or nothing" (significant or not significant) but also the smaller value of threshold for which the result $\underline{y}$ observed will be considered significant that is in theory of the test, the *p-value*.

Being α fixed let a test of level α be defined by a critical region $\Omega_1^{''(\alpha)}$. It is more interesting to take into account to what level will be the results always appear significant. We will use a new index of satisfaction, that was study by Merabet H. (2004), and defined for the Bayesian tests, based on the same prior P_Θ, as:

$$\phi(\omega'') = \begin{cases} 0 & if \quad \omega'' \in \Omega_0^{''(\alpha)} \\ 1 - inf\left\{\beta; \omega'' \in \Omega_1^{''(\beta)}\right\} & if \quad \omega'' \in \Omega_1^{''(\alpha)} \end{cases}$$

(5)

A standard situation is that where it exists an application $\psi(\Theta \to \mathbb{R})$ such as $\Theta_0 = \{\theta;\ \psi(\theta) \le t_0\}$ and where it also exists $\xi(\Omega'' \to \mathbb{R})$ and $g(]0,1[\to \mathbb{R})$ such that

$$\Omega_1^{''(\alpha)} = \{\omega'';\ \xi(\omega'') \le g(\alpha)\}$$

Where $g(\alpha)$ is the $(1-\alpha)$ fractile of the distribution of ξ when $\psi(\theta_0) = t_0$. It thus appears natural to use the p-value to define the satisfaction indexes that are null if a significant effect is not detected, and in the opposite case are an increasing function of the classical indicator of significance. In this case

$$p(\omega'') = P_{\theta_0}\left(\xi > \xi(\omega'')\right)$$

An index of satisfaction is thus defined naturally as:

$$\phi(\omega'') = \begin{cases} 0 & if \quad \xi(\omega'') \le g(\alpha) \\ L\left(p(\omega'')\right) & if \quad \xi(\omega'') > g(\alpha) \end{cases} \quad (6)$$

Where L is a decreasing function. Let F_{θ_0} be a distribution of ξ at the frontier, i. e., for any θ_0 such as $\psi(\theta_0) = t_0$, the index of satisfaction is defined by:

$$\phi(\omega'') = \begin{cases} 0 & if \quad p(\omega'') \ge 1-\alpha \\ L\left(1 - F_{\theta_0}(\omega'')\right) & else \end{cases} \quad (7)$$

The prediction is then given by:

$$\pi(\omega') = \int_{\{\omega'';\, \xi(\omega'') > g(\alpha)\}} L\left(1 - F_{\theta_0}(\omega'')\right) P^{\omega'}_{\Omega''}(\omega'') \quad (8)$$

3. Application :

We propose to calculate explicitly or numerically the prediction of satisfaction in several exponential models for $L(p) = (1-p)$ when the prior distribution of the unknown parameter θ is non-informative (see Robert, 2006) and in the case of a test of threshold, α where the null hypothesis is of type $\theta \le \theta_0$.

3.1. Poisson Sampling :

Let us suppose that X'_i $(1 \le i \le n)$ and X''_i $(1 \le i \le k)$ are *i.i.d.* normal random variables of Poisson distribution $\mathcal{P}(\theta)$, where θ is unknown.
Then $\omega' = \sum_{i=1}^{n} X'_i$ have a Poison distribution $\mathcal{P}(n\theta)$ and $\omega'' = \sum_{i=1}^{k} X''_i$ have a Poisson distribution $B(k\theta)$. If θ has a non informative prior

$$f(\theta) = \theta^{-1}$$

Then the posterior density of θ given ω' will be

$$f(\theta|\omega') \propto Gamma(\omega', n)$$

And the predictive of ω'' given ω' is

$$\nu(\omega''|\omega') = \frac{\Gamma(\omega' + \omega'')}{\Gamma(\omega')\omega''!} \left(\frac{n}{n+k}\right)^{\omega'} \left(\frac{k}{n+k}\right)^{\omega''}$$

The index of satisfaction is then expressed as:

$$\phi(\omega'') = \begin{cases} 0 & if \quad \omega'' < q_0 \\ \sum_{s=0}^{\omega''-1} e^{-k\theta_0} \frac{(k\theta_0)}{s!} & if \quad \omega'' \ge q_0 \end{cases}$$

Where

$$q_0 = inf\left\{s; \sum_{s=0}^{u-1} e^{-k\theta_0} \frac{(k\theta_0)}{s!} \ge 1-\alpha\right\}$$

And the prediction of satisfaction is given by:

$$\pi(\omega') = \sum_{\omega''=q_0}^{\infty} \left(\sum_{s=0}^{\omega''-1} e^{-k\theta_0} \frac{(k\theta_0)}{s!} \right) \nu(\omega''|\omega')$$

$$= \sum_{\omega''=q_0}^{\infty} \left(\sum_{s=0}^{\omega''-1} e^{-k\theta_0} \frac{(k\theta_0)}{s!} \right) \frac{\Gamma(\omega'+\omega'')}{\Gamma(\omega')\omega''!} \left(\frac{n}{n+k}\right)^{\omega'} \left(\frac{k}{n+k}\right)^{\omega''}$$

3.2.Gamma distribution

Let us suppose that X'_i $(1 \le i \le k)$ and X''_i $(1 \le i \le n)$ are *i.i.d.* normal random variables of Gamma distribution $G(p,\theta)$ where θ is unknown and p is known. Then, $\omega' = \sum_{i=1}^{k} X'_i$ have a Gamma distribution $G(kp,\theta)$ and $\omega'' = \sum_{i=1}^{n} X''_i$ have a Gamma distribution$B(np,\theta)$. Let be $K = kp$ and $N = np$.
If θ has a non informative prior $f(\theta) = \theta^{-1}$. Then the posterior density of θ given ω' will be:

$$f(\theta|\omega') \propto Gamma(K,\omega')$$

And the predictive of ω'' given ω' is:

$$\nu(\omega''|\omega') = \frac{1}{\beta(N,K)} \frac{(\omega'')^{N-1}(\omega')^{K}}{(\omega''+\omega')^{N+K}}$$

The index of satisfaction is then expressed as:

$$\phi(\omega'') = \begin{cases} 0 & if \quad \omega'' < q_0 \\ F(\omega'') = \int_0^{\omega''} \frac{(\theta_0)^N}{\Gamma(N)} t^{N-1} e^{-t\theta_0} dt & if \quad \omega'' \ge q_0 \end{cases}$$

Where $F(q_0) = 1-\alpha$.
And the prediction of satisfaction is given by:

$$\pi(\omega') = \int_{q_0}^{\infty} \left(\int_0^{\omega''} \frac{(\theta_0)^N}{\Gamma(N)} t^{N-1} e^{-t\theta_0} dt \right) \nu(\omega''|\omega') \mathrm{d}\omega''$$

$$= \int_{q_0}^{\infty} \left(\int_0^{\omega''} \frac{(\theta_0)^N}{\Gamma(N)} t^{N-1} e^{-t\theta_0} dt \right) \frac{1}{\beta(N,K)} \frac{(\omega'')^{N-1}(\omega')^{K}}{(\omega''+\omega')^{N+K}} \mathrm{d}\omega''$$

This can be estimated numerically.

3.3. Gaussian model

- We will interest ourselves with the Gaussian model because of its central character in experimental sciences and in particular for the clinical trials. The corresponding calculations of the prevision can be realizable by the Monte-Carlo methods.
- We perform independent observations of same normal random variable $\mathcal{N}(\theta,\sigma^2)$. In all that follows, Φ andφ (resp. T_{n-1} and t_{n-1}) indicates the cumulative distribution function and the density of the distribution $\mathcal{N}(0,1)$ respectively (resp. of the student distribution $\mathcal{T}_1(n-1,0,1)$) .
- The first result; $\underline{x} = (x_1, x_2, \dots, x_n)$, is a series of n observations and the second result is a series; $\underline{y} = (y_1, y_2, \dots, y_k)$.
- For obvious reasons of exhaustiveness we will base all calculations on $x = \frac{1}{n}\sum_{i=1}^{n} x_i$ and $y = \frac{1}{k}\sum_{j=1}^{k} y_j$, of distributions $\mathcal{N}(\theta,{\sigma_1}^2)$ and $\mathcal{N}(\theta,{\sigma_2}^2)$, respectively, where ${\sigma_1}^2 = \frac{\sigma^2}{n}$ and ${\sigma_2}^2 = \frac{\sigma^2}{k}$.
- We suppose here that σ^2 is unknown (so ${\sigma_1}^2$ and ${\sigma_2}^2$). We choose as a priori distribution for (θ,σ^2) the non-informative distribution $\pi(\theta,\sigma^2) = \frac{1}{\sigma}$ (See Robert, 2006). We wish to test a null assumption of type $\theta \le \theta_0$.
- We use here a usual test ranging on $\underline{y}$, whose critical region is $]q_0, +\infty[$, where $q_0 = \theta_0 + \sigma_2 u_\alpha^+$, u_α^+ indicating the upper α quartile of the standard normal distribution $\mathcal{N}(0,1)$: $\Phi(u_\alpha^+) = 1-\alpha$.The posterior density associated to the prior $\pi(\theta,\sigma^2) = \frac{1}{\sigma}$ and applied to the second phase $\underline{y} = (y_1, y_2, \dots, y_k)$ is then:

$$\theta \left| \sigma, y, {S_2}^2 \sim \mathcal{N}\left(y, \frac{\sigma^2}{k}\right) \right. and \ \sigma^2 \left| y, {S_2}^2 \sim \mathcal{IG}\left(\frac{k-1}{2}, \frac{{S_2}^2}{2}\right)\right.$$

Where $y = \frac{1}{k}\sum_{j=1}^{k} y_j$ and ${S_2}^2 = \frac{1}{k}\sum_{j=1}^{k}(y_j - y)^2$. And the predictive density of y given x is given by:

$$f_x(y) = \frac{\Gamma\left(\frac{n}{2}\right)}{\sqrt{\pi}\Gamma\left(\frac{n-1}{2}\right)} \frac{1}{\frac{S_1}{\sqrt{\frac{nk}{n+k}}}} \left(\frac{(y-x)^2}{\frac{S_1^2}{\frac{kn}{(n+k)}}} + 1 \right)^{-\frac{n}{2}}$$

Where ${S_1}^2 = \frac{1}{n}\sum_{i=1}^{n}(x_i - x)^2$.

We identify a student distribution $\mathcal{T}_1\left(n-1, x, \frac{S_1}{\sqrt{\frac{nk}{n+k}}}\right)$.

Finally the prevision of satisfaction is:

$$\pi(x) = \int_{q_0}^{+\infty} \Phi\left(\frac{y-\theta_0}{\frac{S_2}{\sqrt{k}}}\right) \times \frac{\Gamma\left(\frac{n}{2}\right)}{\sqrt{\pi}\Gamma\left(\frac{n-1}{2}\right)} \frac{1}{\frac{S_1}{\sqrt{\frac{nk}{n+k}}}} \left(\frac{(y-x)^2}{\frac{S_1^2}{\frac{kn}{(n+k)}}} + 1 \right)^{-\frac{n}{2}} dy$$

3.3.1. Monte Carlo's Method

In order to carry out the calculation of $\pi(x)$ using a Monte Carlo method, and by change of variable, we rewrite it in the following form:

$$\pi(x) = [1 - T_{n-1}(a + \gamma u_\alpha^+)] \int_{-\infty}^{+\infty} \Phi\left(\frac{z - a}{\gamma}\right) \times \frac{t_{n-1}(z)}{1 - T_{n-1}(a + \gamma u_\alpha^+)} \mathbb{I}_{[a+\gamma u_\alpha^+, +\infty[} dz$$

Where $a = \frac{\sqrt{n-1}}{S'_1}(\theta_0 - x)$, $\gamma = \sqrt{n-1}\frac{S'_2}{S'_1}$ with $S'_1 = \frac{S_1}{\sqrt{\frac{nk}{n+k}}}$, $S'_2 = \frac{S_2}{\sqrt{k}}$ and $\frac{t_{n-1}(z)}{1-T_{n-1}(a+\gamma u_\alpha^+)} \mathbb{I}_{[a+\gamma u_\alpha^+, +\infty[}$ is the probability density Q deduced from the cumulative distribution function of the student distribution by conditioning by the event $[a + \gamma u_\alpha^+, +\infty[$.
The Monte Carlo method then consists in approaching $\pi(x)$by:

$$[1 - T_{n-1}(a + \gamma u_\alpha^+)] \left[\frac{1}{N}\sum_{i=1}^{N} \Phi\left(\frac{Z_i - a}{\gamma}\right)\right]$$

Where the Z_i are N realisations of the probability Q. The pulling of the Z_i proceeds in the following way:

- U_i is drawn according to the uniform distribution on$[0,1]$.
- $V_i = T_{n-1}(a + \gamma u_\alpha^+) + \left(1 - T_{n-1}(a + \gamma u_\alpha^+)\right)U_i$; *i.e.,* that V_i follows the uniform distribution on $[T_{n-1}(a + \gamma u_\alpha^+), 1]$.
- $Z_i = {T^{-1}}_{n-1}(V_i)$, i.e., that Z_i follows the distribution Q.

3.3.2. Result's representation :

One will find below the representative curves of π as a function of the number of Monte Carlo samples. We have considered only the case $\theta_0 = 0$ and in the first as in the second sample, the observations are of the same unit variance $\sigma^2 = 1$, considering that a modification of θ_0 and σ^2 will only result in a translation. We have considered the two cases: when $\alpha = 0.05\ and\ \alpha = 0.01$. In other hand, we have taken $k = 30$ and $n = 40\ or\ n = 50$.

- The graphs (1- 2) represent the prevision of satisfaction when $\alpha = 0.05$. The first one is for $n = 40$ and the second is for $n = 50$. We see clearly that the satisfaction augment with n.
- The graphs (3- 4) represent the prevision of satisfaction when $\alpha = 0.05$, also for $n = 40\ and\ n = 50$ respectively. We observe the same remark but the values are reduced.
-

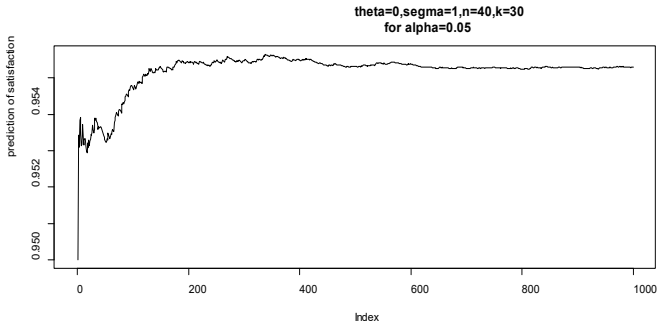

Fig. 1: Convergence of a Monte Carlo sequence for the predictive index of satisfaction based on 1000 iterations, for $\alpha = 0.05\ and\ n = 40$.

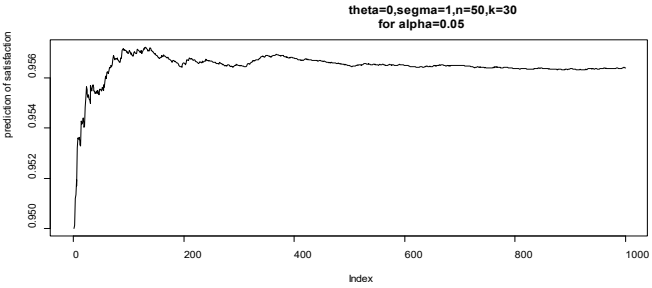

Fig. 2: Convergence of a Monte Carlo sequence for the predictive index of satisfaction based on 1000 iterations for $\alpha = 0.05\ and\ n = 50$.

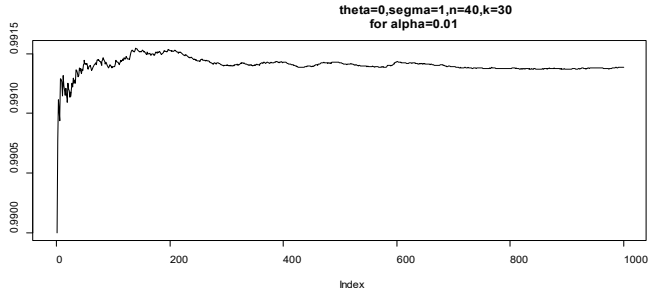

Fig. 3: Convergence of a Monte Carlo sequence for the predictive index of satisfaction based on 1000 iterations for $\alpha = 0.01\ and\ n = 40$.

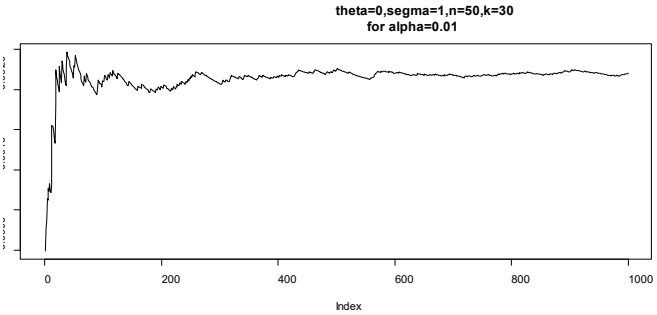

Fig. 4: Convergence of a Monte Carlo sequence for the predictive index of satisfaction based on 1000 iterations $\alpha = 0.01\ and\ n = 50$.

CONCLUSION

The main object of this paper is to chow the important role of the Bayesian predictive procedure applied to a family of limited indices of satisfaction introduced by H. Merbet (2004) which was the generalization of the "rudimentary" index of satisfaction considered by Grouin (1994).

The methodology is useful in two-steps testing procedures, such as those considered in the clinical trials context. The result of the first step is used to decide if the experiment will be continued. Given the posterior distribution derived from the available data, the prevision of satisfaction is defined like the predictive expectation of the index of

satisfaction for the future sample (the interpretation of the index being left to the expert). We consider different cases of the application of the proposed procedure with a non-informative prior.

Bayesian clinical trial simulation is a generic tool that can compute the predictive satisfaction for any trial result, whether that is based on a Bayesian analysis of the data, frequentist significance tests or a formal decision analysis such as a decision by a health care provider to put a drug in the market. In our paper, we have taken an inferential problem related to the Gaussian model.

REFERENCES:

[1] Chow, S. C., 2005. Statistical consideration of adaptive methods in clinical development. Journal Biopharm Stat, 15, 575-91.
[2] Chow, S. C. and al., 2011. Bayesian adaptive methods for clinical trials. Chapman &Hall/CRC Press, New York. ISBN: 978-1-4398-2548-8.
[3] Chow, S. C. and al., 2012. On the independence of data monitoring committee in adaptive design clinical trials. Journal of biopharmaceutical statistics; 22(4):853-867.
[4] Chow, S. C. and Chang M., 2007. Adaptive design in clinical trials. Chapman & Hall/CRC. Biostatistics Series, USA. ISBN: 1-58488-776-1.
[5] Guosheng, Y. and al., 2012. Phase II trial design with Bayesian adaptive randomization and predictive probability. Royal statistical society: Series C (Applied statistics), 61, 219-235.
[6] Hoff, P.D., 2009. A first course in Bayesian statistical Methods. Springer science + Business media, New York. ISBN: 978-0-387-92299-7.
[7] Lee, J.J. and Liu, D.D., 2008. A predictive probability design for phase II cancer clinical trials. Clinical trials; 5:93-106.
[8]Merabet, H., 2004. Index and prevision of satisfaction in exponential models for clinical trials. Statistica, anno LXIV, n3, 441-453
[9] Robert, C.P., 2006. Le choix Bayesien; principe et pratique. Springer-Verlag France, Paris. ISBN: 978-2-287-25173-3.